Copyright Warning & Restrictions

The copyright law of the United States (Title 17, United States Code) governs the making of photocopies or other reproductions of copyrighted material.

Under certain conditions specified in the law, libraries and archives are authorized to furnish a photocopy or other reproduction. One of these specified conditions is that the photocopy or reproduction is not to be "used for any purpose other than private study, scholarship, or research." If a, user makes a request for, or later uses, a photocopy or reproduction for purposes in excess of "fair use" that user may be liable for copyright infringement,

This institution reserves the right to refuse to accept a copying order if, in its judgment, fulfillment of the order would involve violation of copyright law.

Please Note: The author retains the copyright while the New Jersey Institute of Technology reserves the right to distribute this thesis or dissertation

Printing note: If you do not wish to print this page, then select "Pages from: first page # to: last page #" on the print dialog screen

ABSTRACT

ANALYSIS OF 320X240 UNCOOLED MICROBOLOMETER FOCAL PLANE ARRAY AND DESIGN OF THERMOELECTRIC COOLER CONTROLLER

by
Takayoshi Fukaya

Uncooled microbolometer focal plane array is one of the promising method used in uncooled infrared imaging projects. The array's advantages over the conventional cooled imagers are its ability to operate without cryogenic cooler or dewar and its low cost. For the past several years, the ULTRA (Uncooled, Low cost, Technology Reinvestment Alliance) Consortium has been developing uncooled microbolometer imaging system.

This thesis investigates the technology behind the ULTRA camera system. The theoretical as well as the operation of the uncooled microbolometer focal plane array and the processing hardware and software is analyzed and explained.

Thermoelectric cooler controller for the microbolometer focal plane array is designed and described. The thermoelectric cooler, a solid state heat pump, is used to stabilize the temperature inside the microbolometer array packaging at a constant temperature to obtain higher microbolometer performance. The controller is designed and simulated to stabilize minimum of 20mK change in temperature inside the packaging.

ANALYSIS OF 320X240 UNCOOLED MICROBOLOMETER FOCAL PLANE ARRAY AND DESIGN OF THERMOELECTRIC COOLER CONTROLLER

by
Takayoshi Fukaya

A Thesis
Submitted to the Faculty of
New Jersey Institute of Technology
in Partial Fulfillment of the Requirements for the Degree of
Master of Science in Electrical Engineering

Department of Electrical and Computer Engineering

May 1997

APPROVAL PAGE

ANALYSIS OF 320X240 UNCOOLED MICROBOLOMETER FOCAL PLANE ARRAY AND DESIGN OF THERMOELECTRIC COOLER CONTROLLER

Takayoshi Fukaya

Dr. Edwin Hou, Thesis Advisor — Date
Associate Professor of Electrical and Computer Engineering, NJIT

Dr. Nuggehalli M. Ravindra , Committee Member — Date
Associate Professor of Physics, NJIT

Dr. Timothy Chang, Committee Member — Date
Associate Professor of Electrical and Computer Engineering, NJIT

BIOGRAPHICAL SKETCH

Author: Takayoshi Fukaya

Degree: Master of Science

Date: May 1997

Undergraduate and Graduate Education:

- Master of Science in Electrical Engineering,
  New Jersey Institute of Technology, Newark, NJ, 1997

- Bachelor of Science in Electrical Engineering,
  New Jersey Institute of Technology, Newark, NJ 1995

Major: Electrical Engineering

Presentations and Publications:

T. Fukaya, Y. Cai, T. Golota, K. Linga, S. Ziavras, and D. Misra, "VHDL Modeling of the BLITZEN Massively Parallel Processor (MPP)," accepted to Mid-Atlantic Region Local Users Group conference, May 24, 1996, Baltimore, Maryland.

J. Li, T. Fukaya, W.F. Kosonocky, G.H. Olsen, M.J. Cohen, and M.J. Lange, "Development of 3-Color InGaAs FPA Demonstration System," accepted to the 5th Annual Conference of the Society for Imaging Science and Technology, 18-23 May 1997, Cambridge, Massachusetts.

This thesis is dedicated to
my family and Dr. W. F. Kosonocky

ACKNOWLEDGMENT

I would like to express my deepest gratitude to my late advisor Dr. Walter Kosonocky and my advisor Dr. Edwin Hou for giving me the opportunity to work on the research and for their valuable help, guidance, and support. Special thanks to Dr. Nuggehalli M. Ravindra and Dr. Timothy Chang for participating on my committee.

I am grateful to the engineers at Inframetrics for their timely supervision and help. I also wish to thank the other colleagues of the Electronic Imaging Center for their help and friendship, Jun Li, Taras Golota, Zeynep Pektas, Michael Kaplinsky, Dr. Guang Young, and Rakesh K. Kabra.

I would like to acknowledge the financial support received during my graduate study from distinguished late professor Walter F. Kosonocky, the NJIT Foundation Chair for Optoelectronics and Solid State Circuits.

TABLE OF CONTENTS

LIST OF FIGURES

LIST OF FIGURES
(Continued)

Figure **Page**

CHAPTER 1

INTRODUCTION

In recent years, the interest toward uncooled infrared imaging has grown significantly due to its low cost and its ability to operate without cryogenic cooling devices. Microbolometer is one of the successful method used in uncooled imaging projects.

In this thesis, the theory as well as the operation of the microbolometer camera system developed by the Uncooled, Low cost, Technology Reinvestment Alliance project is investigated. The camera system includes focal plane array, processing hardware and software, and each part of the camera is analyzed and described.

The research work also involved designing of the thermoelectric cooler controller which regulates the temperature of the microbolomter at a constant temperature. The temperature stability is an important factor in the focal plane array performance.

This thesis is divided into two parts. The first part describes the theory and the operation of the microbolometer camera system (chapter two and chapter three). The second part is the design of thermoelectric cooler controller (chapter four). Chapter one describes the introduction and background of the microbolometer camera. Chapter two describes the theory and operation of the microbolometer focal plane array. Chapter three discusses about the camera hardware and software. Chapter four describes the controller for the thermoelectric cooler and chapter five is the conclusion.

1.1 Background

For the past several years, the ULTRA (Uncooled, Low cost, Technology Reinvestment Alliance) Consortium has been developing uncooled microbolometer imaging system with its goal to manufacture and sell the system for military and industrial applications. The alliance of ULTRA Consortium consists of Honeywell Technology Center of Honeywell Incorporated, the Autonetics Missile Systems Division of Rockwell International Corporation, Inframetrics Incorporated, and the New Jersey Institute of Technology. A specific task is assigned to each of the group in the development of the microbolometer imaging system. ULTRA has been funded by DARPA sponsored Technology Reinvestment Program grant and by corporate funding.

Honeywell, the primary developer of the VOx microbolometer Uncooled Focal Plane Array (UFPA), has been transferring the microbolometer technology to Rockwell. Rockwell, with its over twenty years of IRFPA design, fabrication, and packaging experiences, has been developing U3000 (microbolometer UFPA), and has developed an enhanced CMOS 320 x 240 multiplexer readout circuit for the array. Rockwell has silicon Micro-Machined Device fabrication line, where the processes and equipment used in the plant are applicable to microbolometer fabrication. A reliable low cost UFPA readout circuit is provided by Rockwell's Semiconductor Systems division, which is a world class commercial silicon CMOS IC producer [10]. Inframetrics, with the goal of incorporating the uncooled technology into its product line, has been working for several years to develop a camera hardware and software platform for the uncooled focal plane arrays. NJIT has been developing a Multi-Wavelength Imaging Pryometry system for the uncooled microbolometer sensor [3].

Figure 1.1 shows the overall system configuration for the microbolometer camera system consisting of optics, the focal plane array, a processing hardware, and a computer.

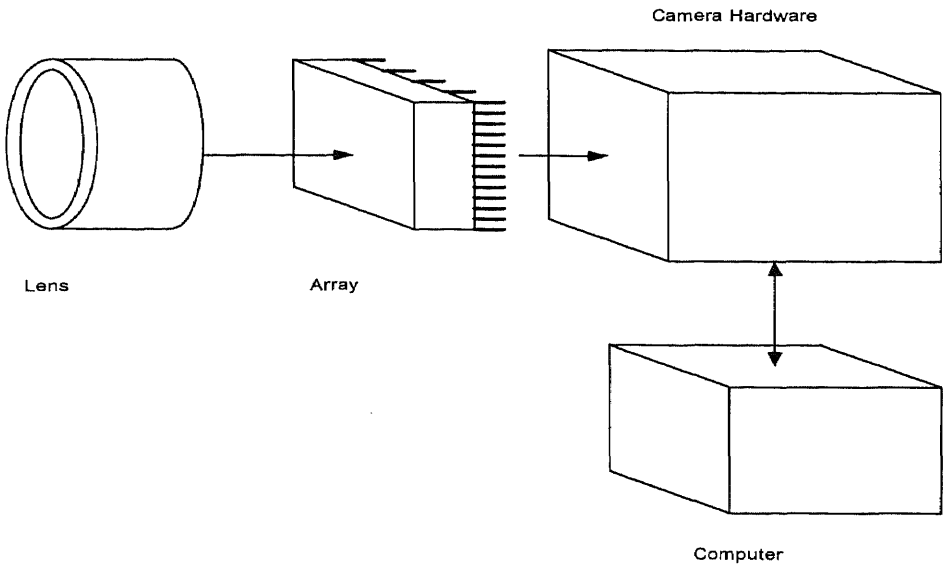

Figure 1.1 *System configuration for the microbolometer imaging system.*

The microbolometer is one of the alternate method for uncooled infrared camera. With government and internal funding, the microbolometer project has been developing at Honeywell Sensor and System Development Center in Minneapolis since 1980's. The project development has been administered by the Army CECOM Center for Night Vision and Electro-optics under the High-Density Array Development (HIDAD) Program.

The concept of the microbolometer is to create an array of bolometers with readout electronics on a single chip to make an imaging device. The bolometer itself is not a new technology. However, the concept of microbolometer has started to emerge due to advances in technology, especially in the area of micromachining.

The conventional infrared cameras use cryogenically cooled photon detecting focal plane array (FPA) that require cooling down to around or below liquid nitrogen temperature, which is about 77K. The cooling of the FPA is due to the relatively large. dark current noise (thermally generated carriers in the semiconductor detector material) at room temperature and also to achieve high sensitivity. The detectors need a dewar or a cryogenic cooler to cool the FPA, making the camera more expensive, heavier, and larger The infrared photon detecting focal plane array require extra processes to fabricate, and it cannot be produced on a standard silicon process line that is available to produce chips today, thus making it expensive.

Microbolometers are designed to overcome these disadvantages of the cooled cameras. Since the microbolometer camera is uncooled, it does not need a dewar or a cryogenic cooler to cool the FPA. This means that it will reduce the cost, the weight, and the size of the camera. Another advantage of the microbolometer is that it does not require extra processes or expensive detector materials to create the focal plane array and can be manufactured on the standard silicon process line. This means that the FPA's can be mass produced and thus their cost are reduced drastically, making infrared microbolometer cameras available to the general public.

As it will be explained later, the bolometer is a radiation power absorbing device which can theoretically detect any wavelength as oppose to cooled photon detecting devices, which has limited detecting bandwidth. The photon detecting devices can only detect a certain window of wavelength according to their energy band gap of the detector material. Since the microbolometer is a radiation power absorbing device, it has a wide dynamic range, meaning capable of detecting in all wavelength. The long-wave infrared

radiation (LWIR) between 8μm to 12μm, popularly used for room temperature radiometric measurements, is the region where the emission of infrared radiation from room temperature objects is the highest. To detect this region with photon sensing devices, expensive materials, such as HgCdTe, are used. On the other hand, microbolometer can be easily modified to observe 8μm to 12μm infrared wavelength range by using filters and by adjusting detector material absorption range.

With the reduction of cost, there are several applications that can benefit from it. For military application, there are applications such as weapon sights for individual soldiers, crew-served weapon sights, sensors for missile seekers, and driver's aides for combat support vehicles. For industrial and commercial application, there are such applications as electric and mechanical troubleshooting, surveillance camera for police and INS, home and business security system, landing aids and traffic monitor for airports and aircrafts, and IR goggles for firefighters [4].

CHAPETER 2

UNCOOLED MICROBOLOMETER FOCAL PLANE ARRAY

2.1 Basic Theory

2.2.1 General Analysis

The bolometer has been in existence for a while. It is a radiation absorbing device which measures the temperature change due to resistance change in a material from the heating effect of the absorbed radiation. Bolometers are power absorbing devices capable of detecting radiation of all wavelengths. One of the application of the bolometer is microwave power measurement where it is usually placed within a microwave waveguide to measure average power. Other applications include power measurement in the audio and radio frequency range.

The most simplest form of bolometer is a short piece of wire. When a piece of wire is radiated with a source, it will heat up due to absorption of radiation. The absorption will cause temperature of the wire to rise, which cause the resistance of the wire to change. The change in the resistance is translated into voltage or current which is proportional to the temperature change.

Figure 2.1 shows a simple model of a bolometer. A mass with thermal capacitance of C is connected to the supporting structure through narrow path with thermal conductance of G. In the case of microbolometer, the thermal conductance path is combined with the electrical conduction path to the readout electronics.

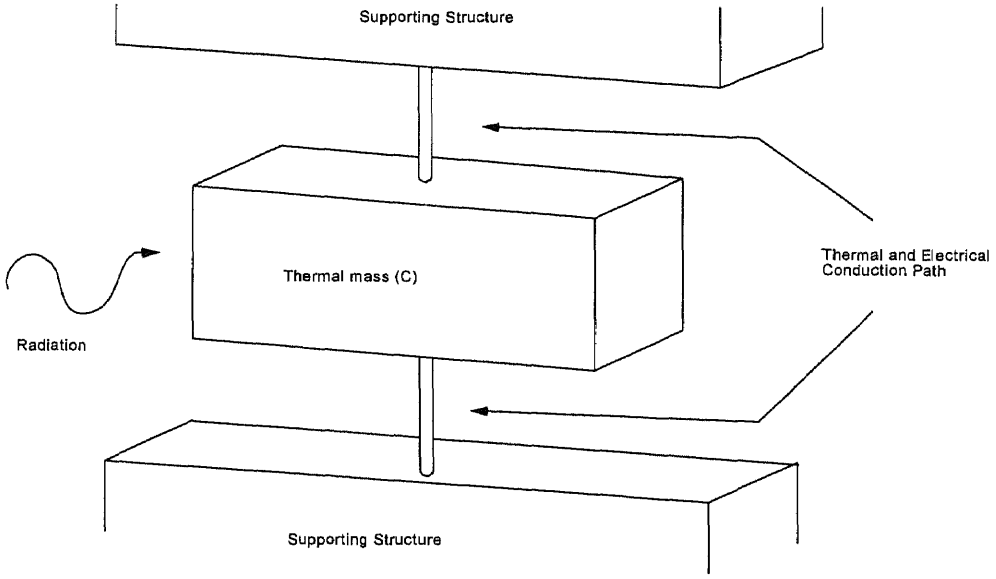

Figure 2.1 *Simplified bolometer structure.*

A mathematical model of bolometer is given in reference [7]. Consider a bolometer system shown in Figure 2.1. The bolometer material has a heat capacity of C and the support structure has a thermal conductance of G. The change in energy, $\Delta\varepsilon$, of the material is proportional to the change in the temperature T. The proportionality constant is the heat capacity of the material. The equation is given by

$$\Delta\varepsilon = C\Delta T. \tag{2.1}$$

The rate of heat flow $\frac{d(\Delta\varepsilon)}{dt}$ is proportional to the change in temperature ΔT with K being the proportionality constant and is given by Equation 2.2.

$$\frac{d(\Delta\varepsilon)}{dt} = K\Delta T = G\Delta T; \tag{2.2}$$

where the proportionality constant K is the thermal conductance G between the detector material and the surrounding.

From Equation 2.1, the rate of heat flow can also be described as

$$\frac{d(\Delta\varepsilon)}{dt} = C\frac{d(\Delta T)}{dt}. \tag{2.3}$$

Assuming the detector material is at higher temperature than the surrounding temperature, the heat flow is from the material to the surrounding. Since the temperature of the material is higher than the surrounding, the rate of heat flow $\frac{d(\Delta\varepsilon)}{dt}$ is negative. With Equations 2.2 and 2.3 equated, the heat transfer equation becomes

$$-C\frac{d(\Delta T)}{dt} = G\Delta T. \tag{2.4}$$

The change in the detector material temperature with the presence of radiation is

$$C\frac{d(\Delta T)}{dt} + G(\Delta T) = \eta P, \tag{2.5}$$

$$P = P_0 \exp(j\omega t);$$

where P is a modulated source power with frequency ω, and η is the detector IR absorption. The value of η depends upon the detector material, the thickness and spacing of the layers, and the pixel fill-factor (the fraction of detecting area to the total area).

The solution to Equation 2.5 is equal to

$$\Delta T = \Delta T_0 \exp(-\frac{G}{C}t) + \frac{\eta P_0 \exp(j\omega t)}{G + j\omega C}. \tag{2.6}$$

The first function of the right hand side of the equation is the transient term and the second function is the periodic term. At steady state, the transient term disappears and the periodic term converges to its steady state magnitude. Equation 2.6 reduces to

$$\Delta T = \frac{\eta P_0}{\sqrt{G^2 + \omega^2 C^2}}. \tag{2.7}$$

The temperature coefficient or thermal coefficient of resistance (TCR) of a material, which describes the material resistance, R_e, variation due to change in temperature, is defined as

$$\alpha \equiv \frac{1}{R_e}\frac{dR_e}{dT}. \tag{2.8}$$

A metal has a linear dependence of change in resistance upon temperature,

$$R_e = R_{e0}[1 + \gamma(T - T_0)]; \tag{2.9}$$

where R_{e0} is the resistance of a material at ambient temperature T_0, T is the absolute temperature, and γ is about 0.5% per degrees Centigrade for many metals [7]. From Equation 2.8, the temperature coefficient of a metal is equal to

$$\alpha = \frac{\gamma}{1 + \gamma(T - T_0)}. \tag{2.10}$$

The resistance dependency upon temperature change and the TCR for a semiconductor are given, respectively, by

$$R_e = R_{e0} \exp(\beta / T), \tag{2.11}$$

$$\alpha = -\beta / T^2; \tag{2.12}$$

where $\beta = \varepsilon_i / 2k$, ε_i is the intrinsic excitation energy or energy band gap, and k is the Boltzmann's constant (1.38×10^{-23} joule/deg K).

There are three types of material that are suitable for the bolometer: metal, semiconductor, and superconductor. Metal and semiconductor bolometers are operated at ambient temperature, but superconducting bolometers need to be cooled down to near absolute zero. Superconductors (lead, tin, tantalum, niobium nitride, and niobium stannide) have a critical temperature, where the resistance of the material below the critical temperature becomes zero, making a sharp change in the resistance near the critical temperature of superconducting material. When operating near the critical temperature, any slight change in the temperature can lead to large resistance change. Superconductors can be used for high sensitivity bolometers.

For metals, the resistance increases with the temperature linearly. In semiconductor material, the resistance decreases as the temperature increases. Therefore, with large bias current applied to a bolometer, the bolometer will eventually burn out. Semiconductor bolometer or thermistor is widely used due to its more pronounced exponential dependence on resistance upon temperature change than the linear metal dependence. For the microbolometer application, semiconductor material is most suitable due to uncooled ambient temperature operation and its resistance characteristics.

Figure 2.2 shows a simple bolometer circuit. The load resistance R_L is in series with the bolometer R_B and the bias voltage source V1. When the circuit is open, the bolometer is at ambient temperature T_0 without radiation and no current flows through the circuit. With the circuit closed and no radiation, the current in the circuit will heat up the bolometer to temperature T_1. The resistance of the bolometer R_B changes to a value

corresponding to T_1. With radiation falling upon the bolometer, the temperature changes by ΔT to a new value T.

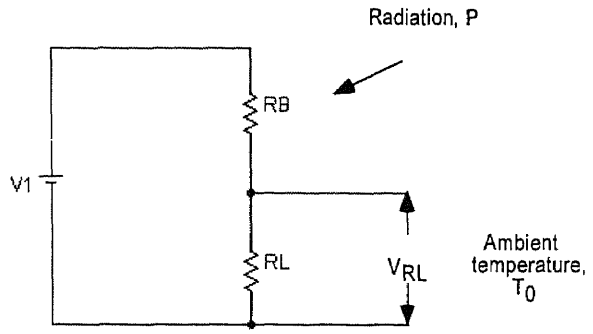

Figure 2.2 *A simple bolometer circuit.*

For the analysis, it is assumed that all the radiation incident upon the detector is absorbed uniformly throughout the volume, the material is uniform throughout the volume, and non-uniform Joulean heating is ignored. In absence of radiation with bias current in the circuit, the heat transfer equation is given by

$$C\frac{dT}{dt} + K_0(T_1 - T_0) = i^2 R_B; \tag{2.13}$$

where K_0 is the average thermal conductance of the medium between the bolometer at T_1 and the surrounding at T_0. The term on the right hand side of the equation is the Joulean heating of the bolometer. With the presence of radiation P, the bolometer changes its temperature by ΔT to T. The heat transfer equation becomes

$$C\frac{d\Delta T}{dt} + K\Delta T = \frac{d(i^2 R_B)}{dT}\Delta T + P; \tag{2.14}$$

where K is the thermal conductance when the bolometer is at T.

The first term on the right hand side can be transformed by substituting i from the circuit,

$$\frac{d(i^2 R_B)}{dT}\Delta T = \frac{d}{dT}\left[\frac{V1^2 R_B}{(R_B + R_L)^2}\right]\Delta T = \frac{V1^2 (R_L - R_B)}{(R_B + R_L)^3}\frac{dR_B}{dT}\Delta T. \tag{2.15}$$

Substituting Equation 2.15 into 2.14 with the definition of temperature coefficient, the equation becomes

$$C\frac{d(\Delta T)}{dt} + K\Delta T = \frac{V1^2 R_B \alpha}{(R_L + R_B)^2}\left(\frac{R_L - R_B}{R_L + R_B}\right)\Delta T + P. \tag{2.16}$$

The Joulean heating in the bolometer in the steady state is related to the conduction losses, which can be expressed as

$$\frac{V1^2 R_B}{(R_L + R_B)^2} = K_0(T_1 - T_0). \tag{2.17}$$

Therefore, Equation 2.16 can be written as

$$C\frac{d\Delta T}{dt} + K_e\Delta T = P; \tag{2.18}$$

where

$$K_e = K - K_0(T_1 - T_0)\alpha\left(\frac{R_L - R_B}{R_L + R_B}\right). \tag{2.19}$$

The solution to Equation 2.18 is Equation 2.6.

If K_e is positive,

$$K > K_0(T_1 - T_0)\alpha\left(\frac{R_L - R_B}{R_L + R_B}\right), \tag{2.20}$$

then the transient term goes to zero with time and the periodic function is left. However, if

$$K < K_0(T_1 - T_0)\alpha\left(\frac{R_L - R_B}{R_L + R_B}\right), \tag{2.21}$$

then the transient term increases exponentially large until eventually the bolometer overheats and burns up. Assuming that R_L is much greater than R_B and thermal conductance stays about the same with change in temperature ($K \approx K_0$), the unstable burn out condition is when

$$\alpha(T_1 - T_0) > 1. \tag{2.22}$$

For metals, where α decreases with temperature (Equation 2.10), it does not meet the condition in Equation 2.22, and self-burnout does not occur. However, in the case of thermistor material, if the bias current is large enough, it will overheat and burnout. The self burnout condition is given by

$$-\frac{\beta}{T_1^2}(T_1 - T_0) > 1. \tag{2.23}$$

The value of β / T_1^2 is about 0.04 for thermistor materials. If the bolometer is at an ambient temperature of 300K, then the critical temperature for self-burnout is about 325K [7].

2.2.2 Responsivity

From the definition of temperature coefficient (Equation 2.8), the change in the bolometer resistance due to change in temperature by ΔT is

$$\Delta R_e = \alpha R_e \Delta T . \tag{2.24}$$

Substituting Equation 2.7 to 2.14, the change in the bolometer resistance equals to

$$\Delta R_e = \frac{\alpha R_e \eta P_o}{\sqrt{(G^2 + \omega^2 C^2)}} . \tag{2.25}$$

With the bias current I_b applied to the circuit, the output signal voltage V_s becomes

$$V_s = \frac{I_b \alpha R_e \eta P_o}{(G^2 + \omega^2 C^2)} . \tag{2.26}$$

The thermal time constant for the bolometer thermal system is given by

$$\tau = \frac{C}{G} . \tag{2.27}$$

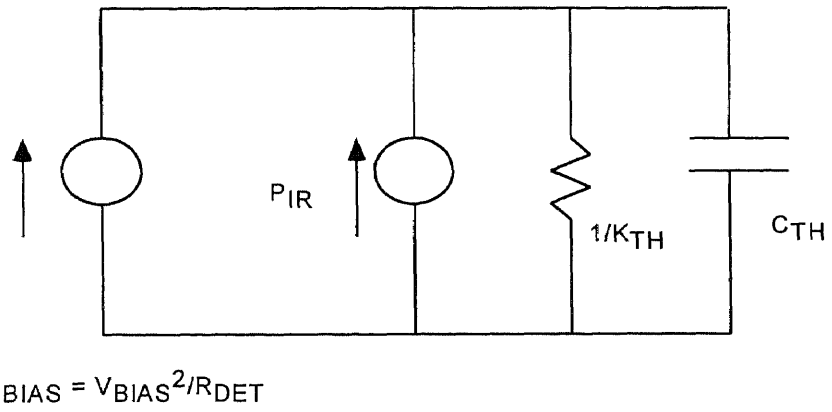

Figure 2.3 *Microbolometer thermal equivalent model.*

Figure 2.3 shows the thermal equivalent model for the microbolometer. The model shows the power input from bias and from the radiation. The thermal time constant can also be derived from this model, which is the same as in Equation 2.27.

The signal voltage (Equation 2.26) in terms of the thermal time constant τ is equal to

$$V_s = \frac{I_b \alpha R_c \eta P_o}{G\sqrt{(1+\omega^2\tau^2)}}. \tag{2.28}$$

The responsivity R is the output signal voltage divided by unit input radiant power,

$$R = \frac{I_b \alpha \mathrm{R_e} \eta}{G\sqrt{(1+\omega^2\tau^2)}}. \tag{2.29}$$

As can be seen from the responsivity equation, to obtain higher responsivity, the bolometer must have a high temperature coefficient and small thermal conductivity G. It is inversely proportional to G at lower modulation frequencies ($\omega\tau<<1$), the region ($\omega \approx$ 8-12μm) where the uncooled thermal infrared detectors are used. The small thermal conductivity G means that the detector must be thermally isolated. In the case of microbolometer, the microbridge or the air-bridge structure provides the large thermal isolation. The higher responsivity is obtained in expense of the thermal time constant. To obtain high responsivity, the response time is slowed down and vice versa. Therefore, the key to develop a "good" bolometer is to have a detecting material with high temperature coefficient α and IR absorption efficiency η, a low thermal capacitance C, and to make the thermal conductance G small as possible [7]. Figure 2.4 shows the response curve for one of Rockwell's U3000 microbolometer array. The typical values for the microbolometer array is listed in Figure 2.5.

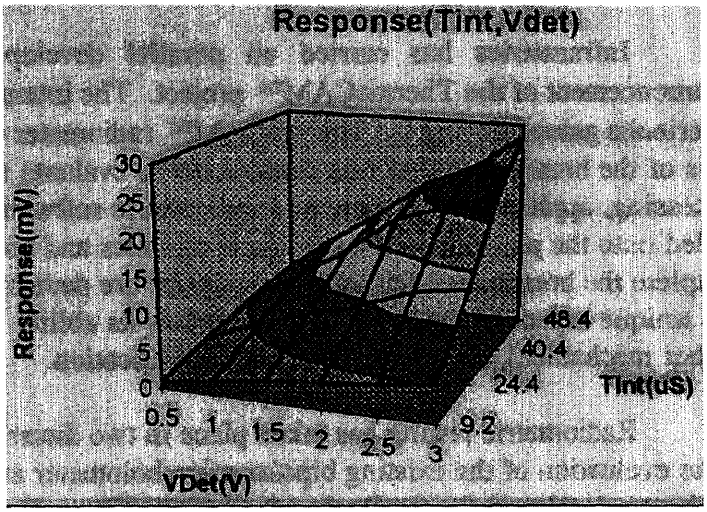

Figure 2.4 *UFPA responsivity for 300K irradiance in the 8 to 13μm* [5].

PARAMETER	DEFINITION	SIGNIFICANCE TO DETECTOR PERFORMANCE	RANGE OF OBSERVED VALUES
TEMPERATURE COEFFICIENT OF RESISTANCE - α_{TH} -	$\alpha_{TH} = R_{DET}^{-1} \partial R_{DET}/\partial T$	SENSITIVITY OF DETECTOR RESISTANCE TO DETECTOR TEMPERATURE CHANGES	0.018 - 0.042 $^{o}C^{-1}$
THERMAL CONDUCTANCE - K_{TH} -	HEAT CONDUCTED PER DEGREE OF ΔT	SENSITIVITY OF DETECTOR TEMPERATURE TO ABSORBED THERMAL RADIATION	1 - 2x10^{-7} WATTS/$^{o}C^{-1}$
HEAT CAPACITY - C_{TH} -	HEAT STORED PER DEGREE OF ΔT	RELATES STORED HEAT TO DEVICE TEMPERATURE	3 - 4x10^{-9} JOULES/$^{o}C^{-1}$
DETECTOR RESISTANCE - R_{DET} -	-	• POWER DISSIPATION • RESISTANCE NOISE	10 - 100 KOHM
DETECTOR RESISTANCE NON-UNIFORMITY - $\delta R_{DET}/(R_{DET})$ -	RATIO OF PEAK-TO-PEAK VARIATION TO AVERAGE RESISTANCE	• RESPONSE AND OFF-SET VARIATIONS • IR DYNAMIC RANGE	2 - 10 %
AREA FILL-FACTOR - Γ -	FRACTION OF TOTAL PIXEL AREA THAT ABSORBS IR	-	0.5 - 0.7
AVERAGE IN-BAND THERMAL EMISSIVITY - ε_{AVE} -	FRACTION OF INCIDENT IR ABSORBED IN-BAND	THE TOTAL IR ABSORPTION EFFICIENCY IS DETERMINED BY THE PRODUCT $\Gamma\varepsilon_{AVE}$	0.8 - 0.85
DETECTOR 1/f NOISE PARAMETER - $k_{1/f}$ -	$\langle \delta V_{1/f}^2 \rangle = k_{1/f} V_{BIAS}^2$ WHERE $\langle \delta V_{1/f}^2 \rangle$ IS THE DETECTOR'S RMS 1/f NOISE VOLTAGE	SETS LOWER LIMITS ON SIGNAL-TO-NOISE RATIO AND CALIBRATION STABILITY	1 - 3x10^{-13} Hz$^{-1/2}$

Figure 2.5 *Typical microbolometer values for U3000 microbolometer array* [5].

2.2.3 Noise

The detection capability of any imaging system is limited by fluctuations of a random nature, noise. There are three categories that the noise appearing in an infrared system may arise from: noise in detectors, in readout electronics, and from the radiation background. In a microbolometer UFPA, there are three primary noise sources to be considered. The Johnson noise of the bolometer, the 1/f noise characteristic of both amorphous and poly-crystalline semiconductors, and the fundamental thermodynamic temperature fluctuation noise of the individual detector elements. Also, there are noise from the readout electronics and the detector bias supply, but the common-mode noise rejection features that are incorporated into Rockwell's design of UFPA effectively suppresses the noises.

The Johnson noise or thermal noise appears in any resistive material. It is caused by the random motions of the charge carriers. 1/f noise or current noise is a dominant noise source of semiconductor materials at low frequencies. The background noise is due to the quasi-random arrival of photons from the surrounding of the detector. The background noise ultimately limits the performance of any thermal detector, because the noise from the background still exists even if all of the other noise is suppressed. Due to statistical nature of the heat interchange with the surrounding, a thermal detector in contact with its environment by conduction and radiation exhibits random fluctuations in its temperature, known as temperature fluctuation noise. The temperature fluctuation noise not only comes from the source background, but also from detector casing, electronics, and even the detector itself.

Noise equivalent temperature difference (NETD) is defined as the temperature difference seen in a large blackbody or between two adjacent large blackbodies by an infrared thermal imaging system, which will give rise to signal to noise ratio of unity in the electrical output of the focal plane array and readout electronics [9]. It is essentially bolometer's sensitivity to temperature change.

Detectivity D^*_{TF} in a temperature fluctuation noise limited detector is equal to

$$D^*_{TF} = \left(\frac{\eta^2 A_D}{4kT_D^2 G} \right)^{1/2}; \tag{2.30}$$

where A_D is the detector area equal to the pixel area in an array, k is the Boltzmann's constant, and T_D is the detector temperature. If the principal thermal loss mechanism is by radiation only, then the temperature fluctuation noise becomes background fluctuation noise, which is the ultimate limit of any thermal detector. The radiant loss can be represented by G_r, the effective thermal conductance

$$G_r = 4\eta\sigma A_D T_B^3; \tag{2.31}$$

where T_B is the background temperature.

Using Equation 2.30 and 2.31, the background limited detectivity is given by

$$D^*_{BF} = \left[\frac{\eta}{8k\sigma(T_D^5 + T_B^5)} \right]^{1/2}; \tag{2.32}$$

where σ is the Stefan-Boltzmann constant [9]. The equation of noise equivalent temperature difference is equal to

$$NETD = \frac{(4F^2 + 1)V_N}{A_D \tau_0 R(\Delta P / \Delta T_s)_{\lambda_1 - \lambda_2}}. \tag{2.33}$$

F is the f/# of the optics, V_N is the electrical noise within the system bandwidth, τ_o is the transmittance of the optics and $(\Delta P / \Delta T)_{\lambda_1-\lambda_2}$ is the rate of change of the radiated power per unit area of a blackbody at temperature T_S measured within the spectral interval from λ_1 to λ_2. The relationship between D^* and responsivity R is defined as

$$D^* = \frac{(A_D B)^{1/2} R}{V_N}; \tag{2.34}$$

where B is the measurement bandwidth.

Substituting Equation 2.30 to Equation 2.33 and with Equation 2.34, the expression for the noise equivalent temperature difference in a temperature fluctuation noise limited imaging array becomes

$$NETD_{TF} = \frac{2(4F^2+1)T_D(kBG)^{1/2}}{\eta A_D \tau_o (\Delta P / \Delta T)_{\lambda_1-\lambda_2}}. \tag{2.35}$$

In similar fashion, combining Equation 2.32 and 2.33 gives the background limited detector NETD,

$$NETD_{BF} = \frac{(4F^2+1)}{\tau_o (\Delta P / \Delta T_s)_{\lambda_1-\lambda_2}} \left[\frac{8k\sigma B(T_D^5 + T_B^5)}{\eta A_D} \right]. \tag{2.36}$$

Figure 2.6 a) and b), respectively, illustrates Equations 2.35 and 2.36, where all thermal infrared detectors must fall on or above the limits shown. With a given value of G, a detector cannot have an NETD better than or points lower than the sloping line. The actual detectors usually lie above the sloping line due to higher noise than that of temperature fluctuation noise. Within the parameters given, no detector can have NETD better than (lower than) the background limit shown.

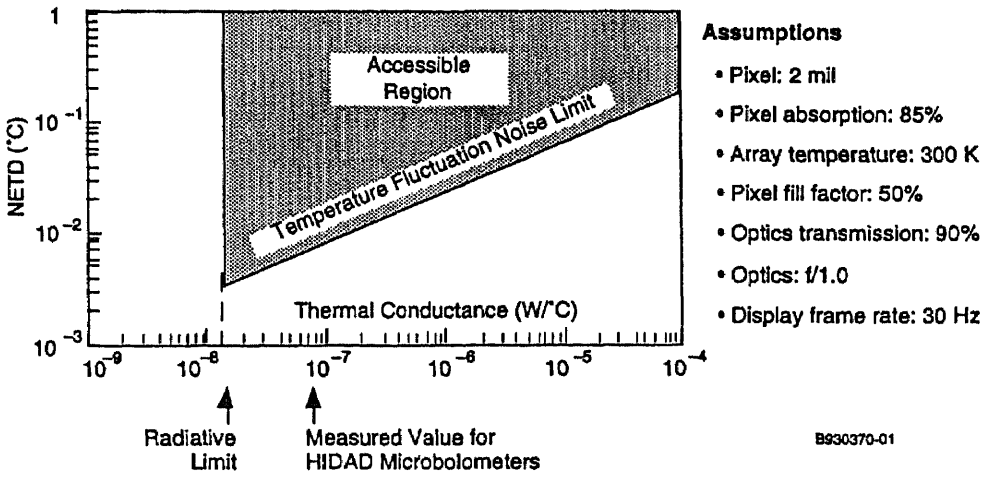

a) *Temperature fluctuation noise limit.*

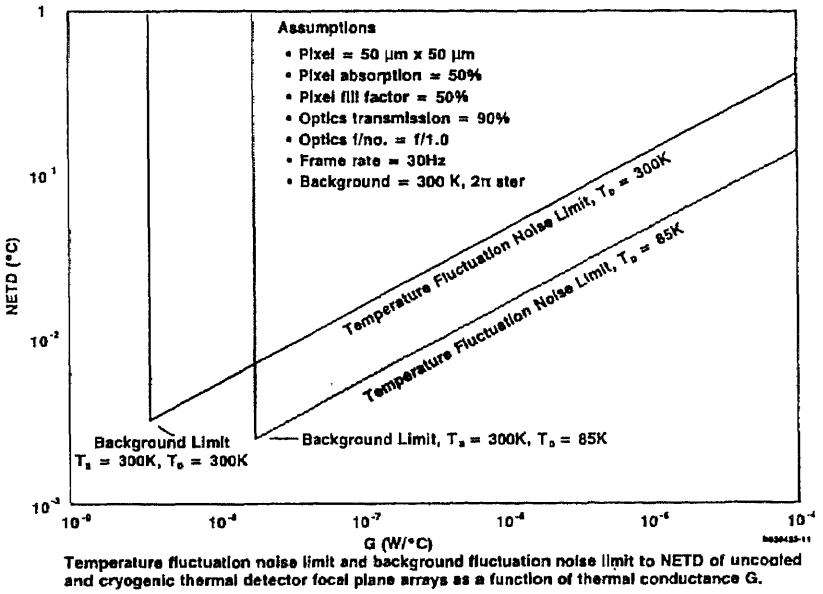

Temperature fluctuation noise limit and background fluctuation noise limit to NETD of uncooled and cryogenic thermal detector focal plane arrays as a function of thermal conductance G.

b) *Temperature and background fluctuation noise limits.*

Figure 2.6 *NETD temperature fluctuation and background fluctuation noise limits* [8].

To obtain the temperature fluctuation noise limited system, the temperature fluctuation noise must be greater than any other noise, including Johnson noise and 1/f power noise. The temperature fluctuation noise limited detector voltage V_{TF} is given by

$$V_{TF} = I_b \alpha R_e \left(\overline{\Delta T^2}\right)^{1/2} = I_b \alpha R_e \left(\frac{kT^2}{C}\right)^{1/2}; \tag{2.37}$$

where I_b is the bias current, α is the temperature coefficient of resistance, R_e is the detector resistance, and the mean square temperature fluctuation noise is equal to

$$\overline{\Delta T^2} = \frac{kT^2}{C}. \tag{2.38}$$

The Johnson noise of any resistive material including the bolometer is

$$V_J = (4kT_D R_e B)^{1/2}. \tag{2.39}$$

The 1/f power noise of the detector is given by

$$V_P = \frac{(KI_b^{\delta} B)^{1/2} R_e}{f^{\beta}}; \tag{2.40}$$

where the K is proportionality factor, f is the frequency, δ and β are coefficients whose values are about two and unity, respectively. Theoretically, the temperature fluctuation noise limited performance is possible, if the bias can be increased sufficiently without overheating the bolometer and without adding 1/f power law noise or raising V_J over V_{TF} [3],[6].

2.2 The UFPA Structure

Figure 2.7 shows the functional architecture of the UFPA. It consists of 320 x 240 unit cells, output multiplexers and driver, horizontal and vertical shift registers, signal

conditioning electronics, timing and control logic, and on chip bias generation and microbolometer overheat protection circuitry.

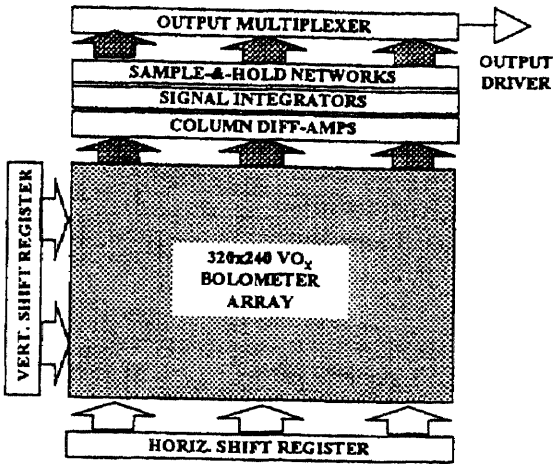

Figure 2.7 320X240 *Microbolometer array structure with readout electronics* [5].

All of the 240 column detector signal path is connected to the signal conditioning network located at the end of each column. The signal conditioning network is comprised of a column differential amplifier, signal integrators, and a sample and hold network. The signals coming out of the 320 sample and hold networks are shifted out to the output driver by the output multiplexers. The U3000 is designed with an on-chip bias generation that generates all the necessary bias voltages to operate the UFPA. If the auto-bias function is turned off, then the bias voltages are to be provided externally. The horizontal and vertical shift registers are used to control the FPA scanning. Also, end-of-line and end-of-frame Build-In Test (BIT) clocks, used by the sensor to verify normal UFPA operation, are generated by the shift registers. The BIT features are designed to

provide protection against detector overheating in case of external clock failures and to furnish the sensor with the UFPA status signals [10].

The focal plane array consists of 320 x 240 microbolometer unit cells, which is formatted for 50% full TV resolution. A unit cell consists of a micro-bridge and readout electronics, which includes detector selection switch transistors, as shown in Figure 2.8. The microbridge structure is fabricated on top of the readout electronics. The first generation of microbolometers, made by Honeywell, used a bipolar transistor for detector selection switch in the readout circuits. The second generation microbolometer readout circuit, the U3000's made by Rockwell, uses MOSFET for their selection switch.

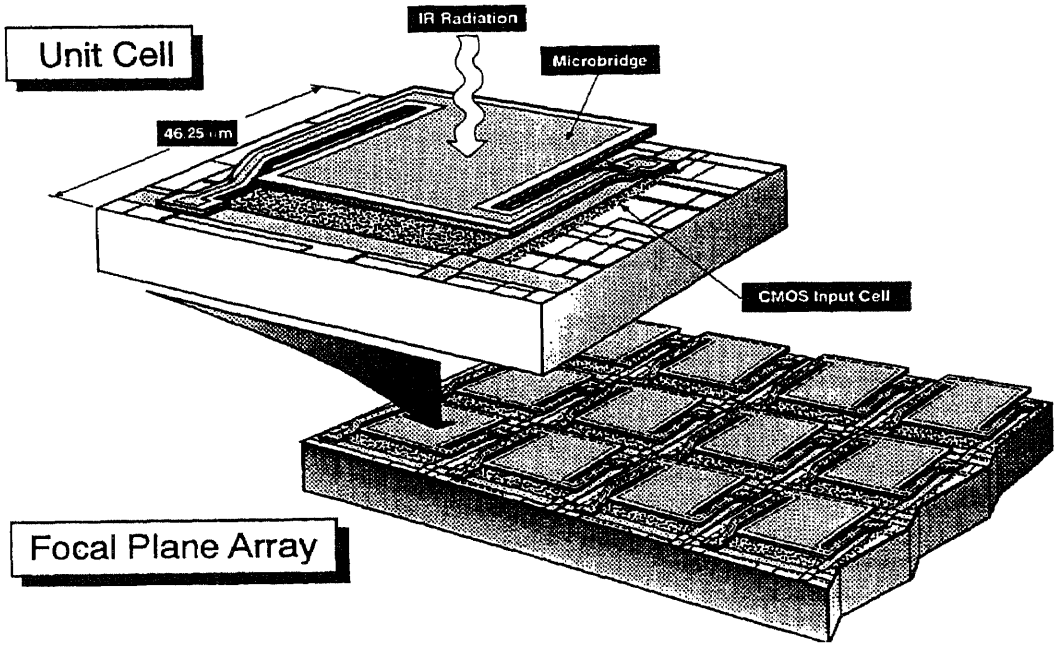

Figure 2.8 *Diagram showing FPA and a unit cell* [8].

Figure 2.10 shows a typical thermal isolation structure of a monolithic VOx microbolometer cell with detector integrated on to an air-bridge. Using standard silicon IC thin film process, the microbolometer thermal isolation structure is deposited directly on top of readout integrated circuit (ROIC) wafers. The two long thin legs that connect each detector to the ROIC substrate provide extremely high thermal isolation necessary for the microbolometer responsivity. The two legs also serve as both thermal and electrical conduction path to the ROIC, which acts as a heat sink for the detector. Deposited metal plugs located at the end of each leg are used for mechanical and electrical contact to the readout circuit [10].

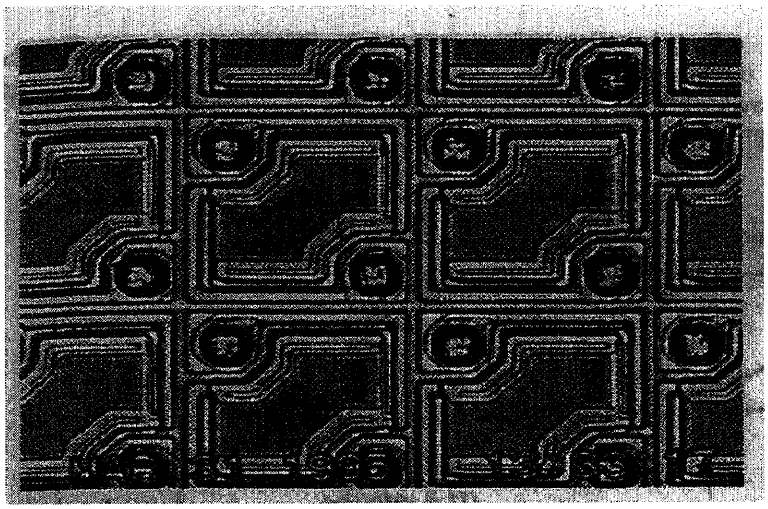

Figure 2.9 *A photograph of microbolometer array.*

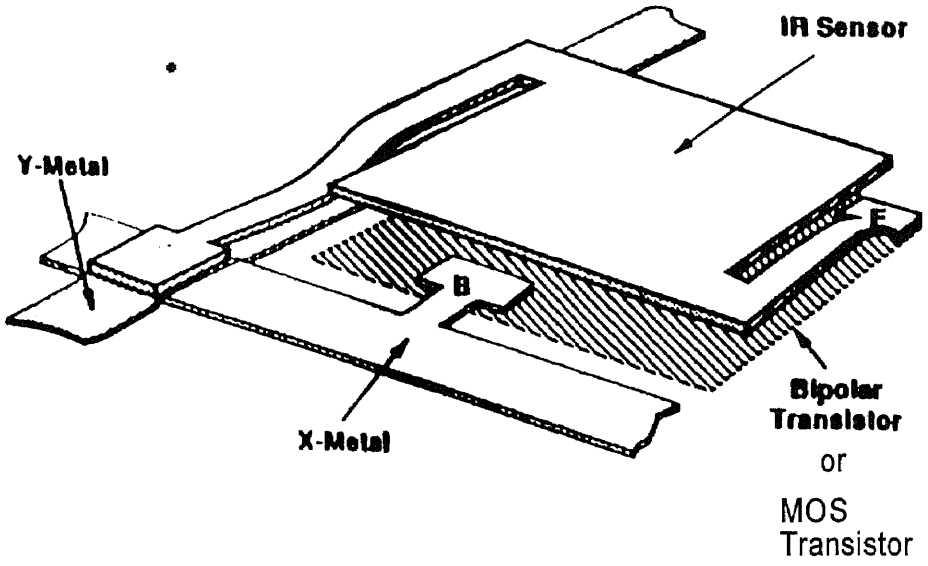

Figure 2.10 *A figure of a microbridge or air-bridge.*

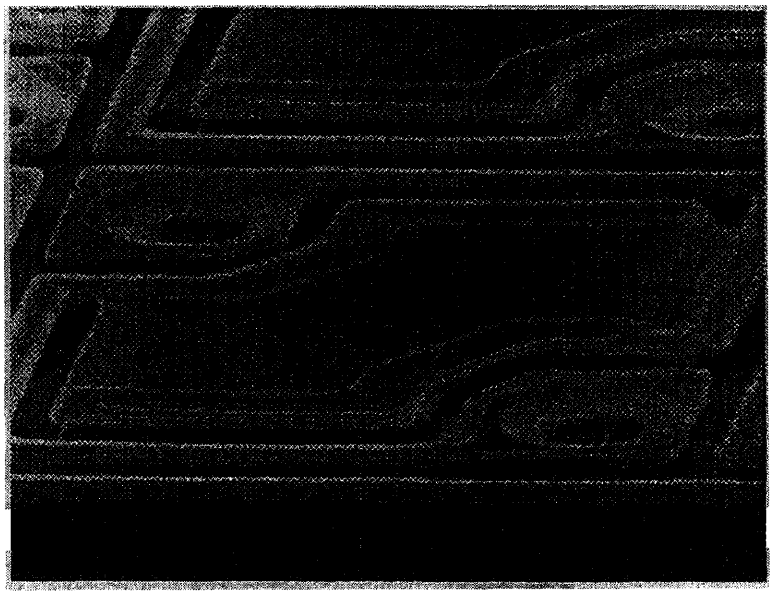

Figure 2.11 *A photograph of a microbolometer unit cell, where the bridge structure is shown.*

The UFPA is packaged inside a vacuum sealed packaging with a thermoelectric cooler. The thermoelectric cooler is used regulate the operating temperature inside the package to compensate for the temperature drift. The array requires moderately high

vacuum to reduce the heat leakage to air. The heat leakage degrades the detector sensitivity by reducing the high thermal isolation of the air-bridge structure. In order for the microbolometer to have high performance, at least 75mT or less is recommended [2].

Figure 2.12 *UFPA packaging* [5].

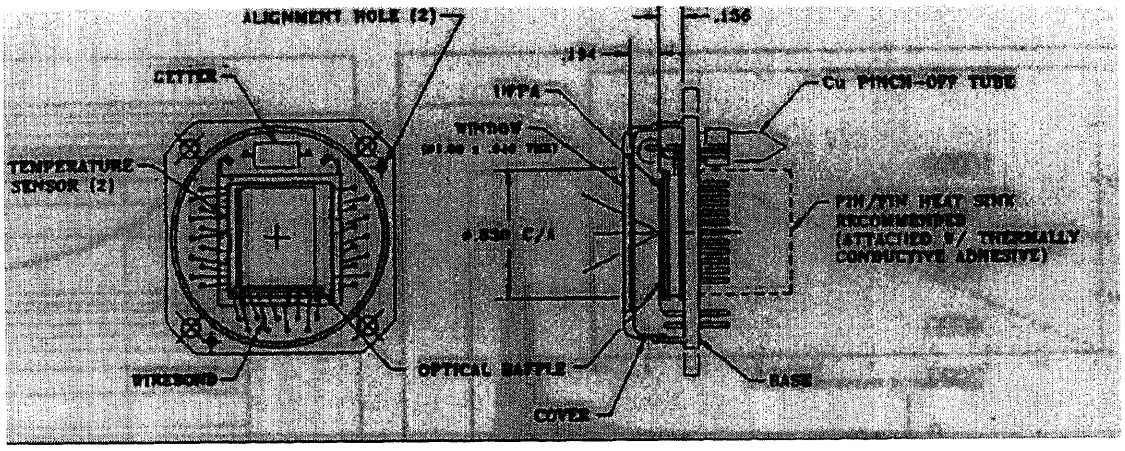

Figure 2.13 *Array package* [5].

The package is assembled and covered with all-metal construction (Figure 2.12). As shown in Figure 2.13, inside the Cu pinch-off tube is a non-evaporable getter provided for continuous pumping and long vacuum life. Mounted on the cover is a two-side Anti-

reflection (AR) coated Ge window which transmits 98% of in-band IR signal. The height of the package is less than 0.5 inches, and lateral dimensions are 1.5 inches.

2.3 Fabrication

As mentioned before, one of the advantage of the microbolometer its production process compatibility with the standard silicon IC process. VOx thermal isolation structure arrays are co-deposited on top of the ROIC wafer using standard silicon IC thin film processing. Through the removal of the sacrificial layer between the thermal isolation structures and the ROIC at the end of the fabrication process, high level of thermal isolation is achieved. The fabrication of the microbolometer involves micromachining techniques. The simplified microbolometer fabrication step are described below [9].

1. All the necessary readout electronics, including transistors and metal inter-connections, are imbedded in a monolithic silicon wafer.
2. Sacrificial layer islands are deposited on top of the readout electronic.
3. Deposit supporting bridge material (silicon nitride).
4. Deposit metal connection for the detecting material.
5. Deposit detector (thermal mass) material (vanadium oxide).
6. Deposit supporting bridge material (silicon nitride).
7. Etch away the sacrificial layer islands.

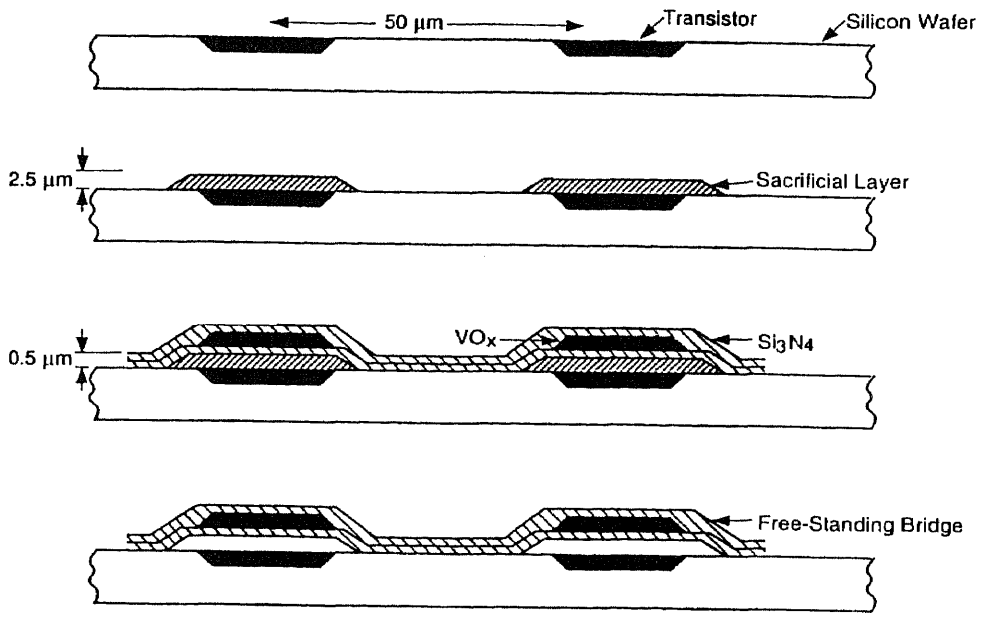

Figure 2.14 *Simplified fabrication steps for the microbridge structure* [9].

An improved and simplified process for the microbridge structure is being developed by Rockwell. With the new process, the number of microbolometer array process steps can be reduced by 30%, and both metalization and dielectric processes are improved. It eliminates two photomask layers and replaces wet-etch with dry-etch process. It is expected that UFPA performance will be improved with the 25% reduction in thermal conductance and a broadening of the spectral response band.

2.4 Timing

The UFPA is design to output a single signal channel that is compatible with both U.S and European (PAL) TV synchronization standards, where the image can be viewed without reformatting the output signal. The output video is TV (60 Hz) compatible RS-

170 synchronization standard signal. The operation of the array is controlled by three external clock pulses; ICLOCK, LSYNC, and FSYNC.

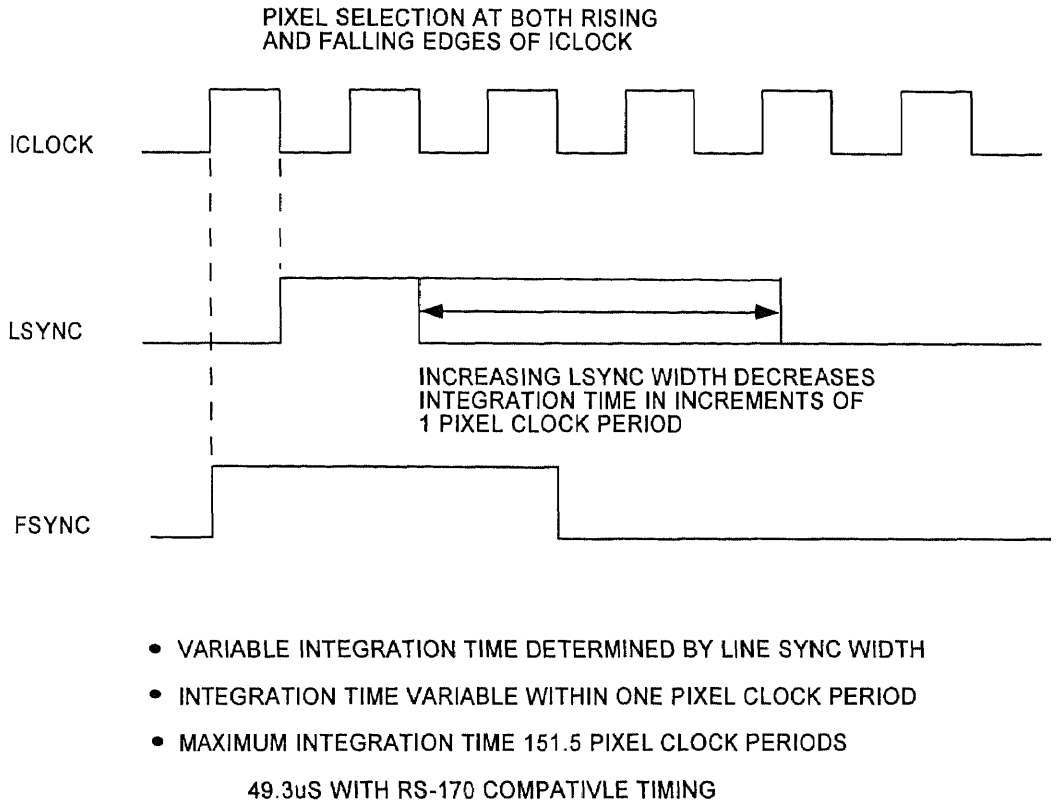

Figure 2.15 *Three external clock to operate UFPA: mater clock ICLOCK, line sync pulse LSYNC, and frame sync pulse FSYNC.*

ICLOCK is the master clock where the readout is synchronized with the clock. LSYNC is a line sync or horizontal sync control pulse which simultaneously controls the signal integration time and detector bias period. The integration time is controlled by the length of LSYNC clock pulse. By increasing the pulse width of the LSYNC, the integration time decreases. Therefore, at the maximum integration time is when the LSYNCE pulse is the shortest, which is equal to 1 clock pulse. With the integration time

control, it is possible for the camera to have a greater dynamic range (see Figure 2.4). It is strongly recommended that the detector integration time does not exceed 50μs to avoid detector overheat and self-burnout. FSYNC is a frame sync or vertical sync pulse, where the frame rate is set by the pulse. The U3000 is design to operate at frame rate of at least 60Hz [5][10].

To readout the detector signal output current (or voltage), bias voltage (or current) is applied to the microbolometer. Since the detector has very small heat capacity and thermal conductance, the detector heats up rapidly. The bias voltage must be applied to each detector for a short period (in a form of pulse) to avoid overheating and thermal run-away. The pulsed biasing causes the detector's electrical signal response to be highly dynamic. Here, the detector's electronic Noise Equivalent Band Width is about 1/(bias pulse time duration). In the readout operation, bias voltage is briefly applied to the detector in each frame, and the detector is permitted to thermally discharge during the remainder of the frame time with thermal time constant of about 10ms [10]. As of today's microbolometer technology, the slow response of the microbolometer makes it unsuitable to be used in systems, such as heat seeking missile sensor that require fast response.

During the operation, an entire row of 320 detectors is operated in parallel. LSYNC selects a row and detector bias is applied for the detector signal readout. The signal integration begins at the falling edge of LSYNC and ends at the beginning of the horizontal blanking period. Also at the beginning of the horizontal blanking period, the

amplified and integrated detector signals are sampled. Readout multiplexing of the sampled detector signals occurs during the next line time [10].

CHAPTER 3

CAMERA HARDWARE

3.1 Design

For the past several years, Inframetrics has been working to incorporate the uncooled technology into its product line. The initial work began with the development of the video head electronics to drive the Honeywell bipolar UFPA. Inframetrics developed the interface board to filter, to sample and hold, and to digitize the bipolar array output. To produce a still frame imaging breadboard, the video head integrated the uncooled array, optics, interface board, and a commercially available frame grabber. Already existing FpaVIEW software, developed by Inframetrics, was expanded to interface the breadboard for testing the Honeywell bipolar array.

Recently, Inframetrics developed ThermaCAM™ imaging radiometer based on the Hughes variable integration time PtSi array. The ThermaCAM™ project goal is to develop a platform for both cooled and uncooled detectors. ThermaCAM™ was designed to provide a standard electronics and software platform for a variety of array formats and detector technologies, specifically the uncooled focal plane arrays. The camera hardware can be divided into two main functional blocks; the FPA interface module and the video processing module.

The FPA interface module provides all the biases, timing pulses, and output signal conditioning, electronically reconfigurable for a particular array being integrated with the sensor, necessary to operate the array. The module digitizes the array output and converts the array readout frame rate with the standard video output frame rate of the video

processing module by a scan converter. To optimize the sensor's performance, array bias and clock levels are individually programmed. The specific timing requirement and the size of the array can be adjusted by programming the timing generator and input buffers.

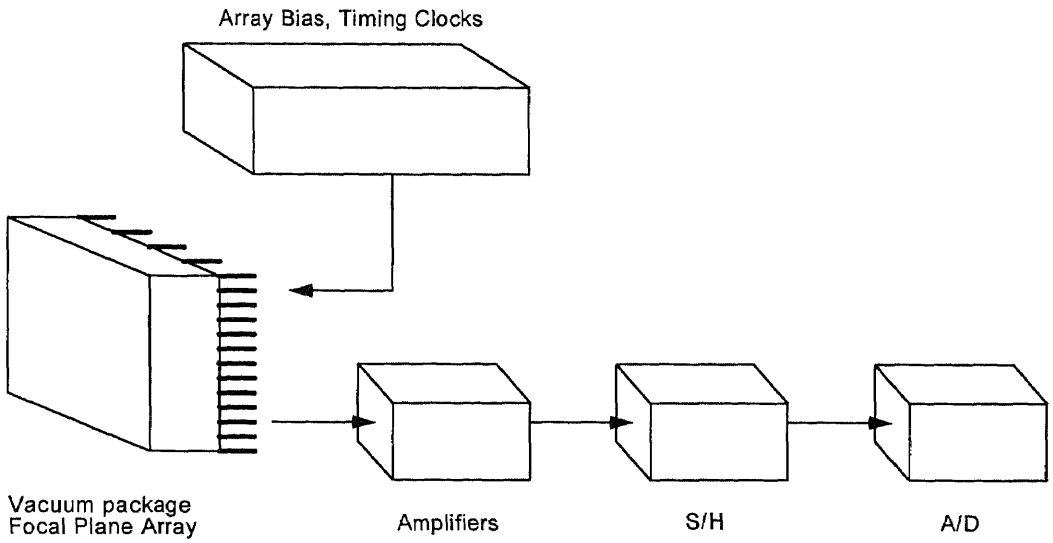

Figure 3.1 *UFPA interface board block diagram.*

The majority of the sensor functions are performed by the video processing module. The tasks include image processing functions of "equalization", or non-uniformity correction, and scaling the dynamic range of the detector to the temperature span of interest. The user interface for measurement modes, temperature spans and ranges, setup menus, colorization, zoom and cursor control is provided by the video processing board also. Mass storage functions on a PCMCIA card as well as a common file format are available for storing and retrieving digitized images into the sensor. For communications protocol, a standard remote control interface to the sensor is maintained.

The module includes colorized output in NTSC or PAL, black and white radiometrically calibrated analog video, and 12 bit digital video output.

The ThermaCAM™ software is applicable to both cooled and uncooled arrays. The process of the software includes "equalization," a standard method of determining correction coefficients in the computer and downloading coefficients back to the camera, to acquire proper frame data for the process. The software functions include file management, live image display, image capture, histograms, NETD, image pixel statistics, gain and offset coefficients, calibration curves, image brightness and contrast, colorization, and several other specialized features.

Inframetrics developed the imaging test fixture for the Honeywell bipolar array by integrating the interface board with ThermaCAM™ electronics. The test fixture allowed preliminary array and radiometric characterization, while the Rockwell arrays and the associated imaging board were being developed. Information gained from the array and radiometirc characterization was used to improve the system for the Rockwell array [5]., A new interface board was developed for the microbolometer arrays to compensate for signal levels and noise characteristics different from that of photon detectors.

Figure 3.2 shows the camera test fixture for the Rockwell microbolometer array. It consists of the new interface board and the ThermaCAM™ platform electronics. Figure 3.3 shows the test fixture functional block diagram. The UFPA array is connected to the interface board with sample and hold, and 16-bit A/D converter. The digitized video is sent to the video processor module for signal processing and also to the computer where the offset correction coefficient calculation is performed. The coefficients are sent back to the interface board for offset correction through D/A.

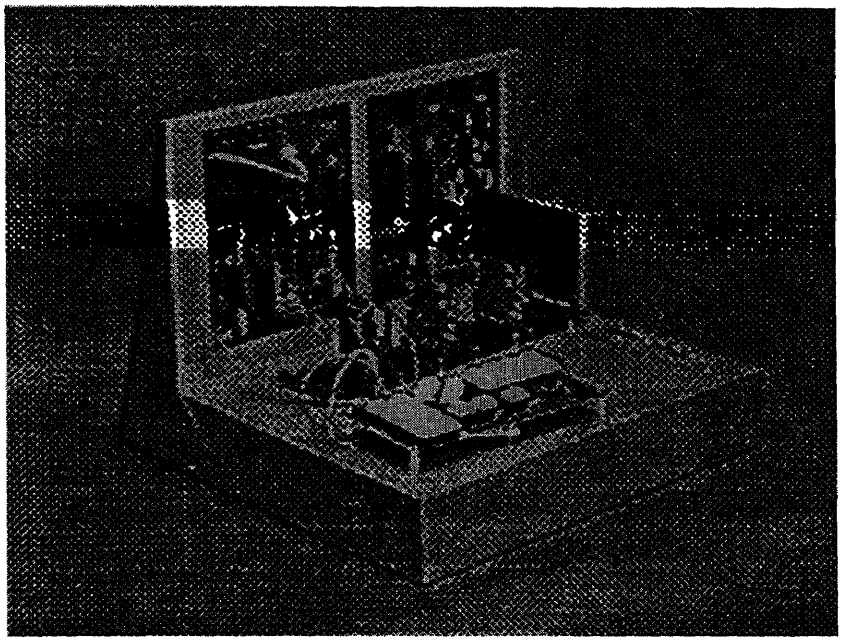

Figure 3.2 *Microbolometer test fixture.*

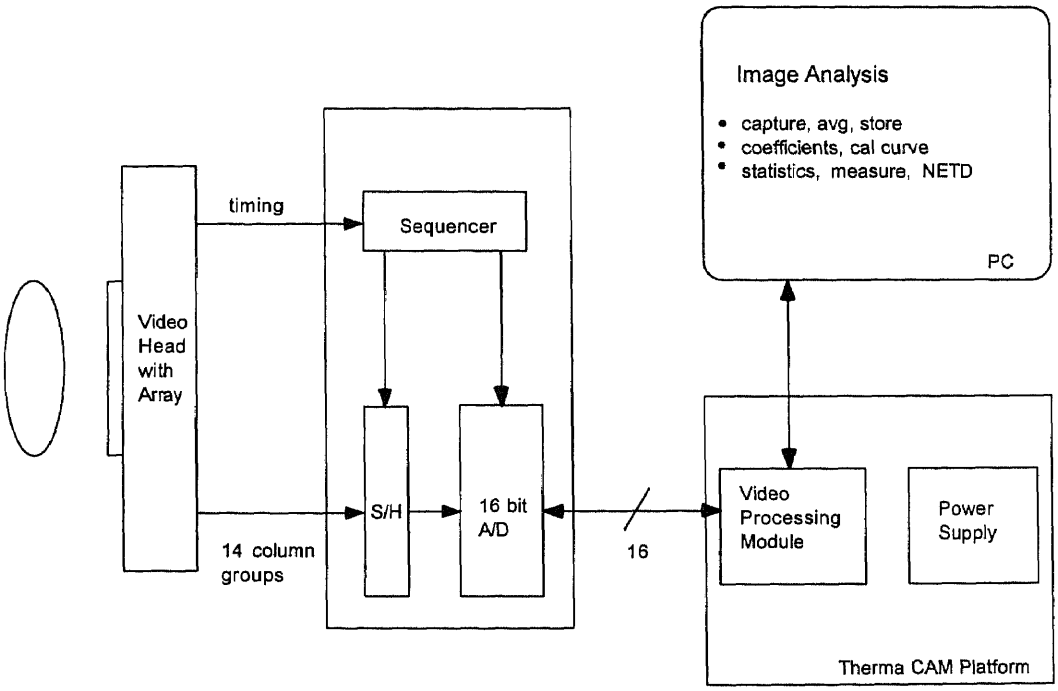

Figure 3.3 *UFPA camera platform.*

CHAPTER 4

THERMOELECTRIC COOLER CONTROLLER

4.1 Thermoelectric Cooler

A thermoelectric module is a device that can be used as a heat pump or as an electrical power generator. It is called an electrical power generator when it is used to generate electricity, and it is called a thermoelectric cooler (TEC) when it is operated as a heat pump. For the purpose of microbolometer temperature stabilization, the module is only needed to operate as a heat pump (thermoelectric cooler).

The thermoelectric module is analogous to that of a standard thermocouple used to measure temperature. Thermocouples are made from two junctions formed by two dissimilar metals, such as copper and constantin. When measuring temperature, one side of the junction is kept at some reference temperature and the other side is attached to the target temperature. The voltage difference created by the junction is related to the temperature difference. The operation is analogous to the thermoelectric module being used as a power generator. On the other hand, applying electrical energy to the junction of thermocouple will cause one junction to become cold and the other to become hot. This is analogous to the thermoelectric cooler operation.

Thermoelectric cooler is based on the concept of the Peltier effect, which was discovered in 1834. The Peltier effect is the change in temperature due to current passing though a junction of two different types of conductor. The thermoelectric cooler uses p-type and n-type semiconductor material (bismuth telluride), connected in series placed between two ceramic plates to optimize electrical insulation and thermal conduction with

high mechanical strength as shown in Figure 4.1. It is a solid state heat pump that has no moving parts, fluids or gasses as in the conventional cooling system.

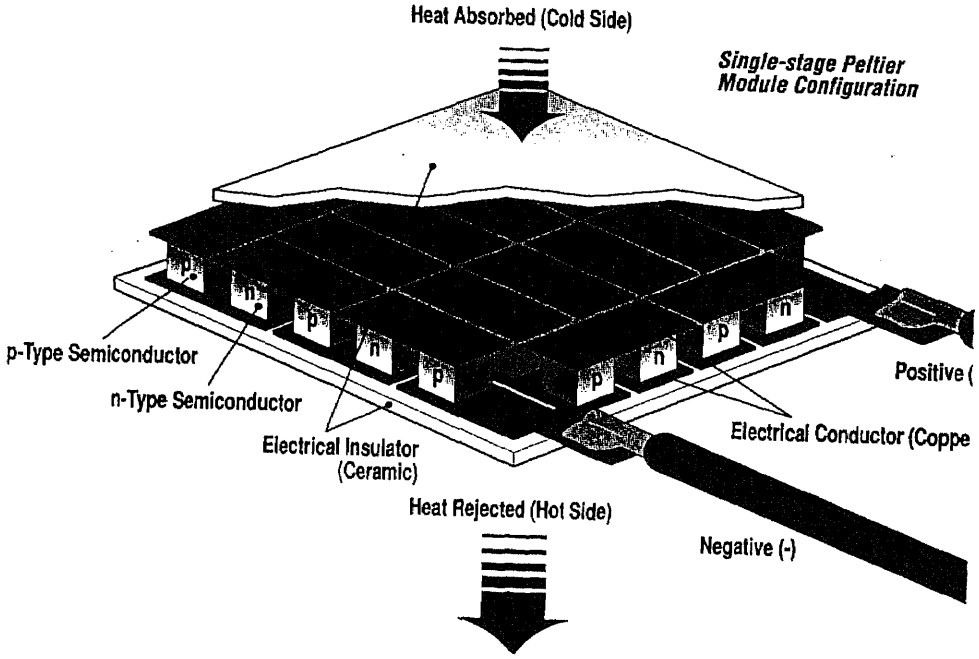

Figure 4.1 *Thermoelectric cooler. Heat is pumped from the cold side to the hot side* [11].

There are three fundamental components to the conventional refrigeration system: the evaporator, the compressor, and the condenser. The evaporator or cold section is used to allow the pressurized refrigerant (freon) to boil, to expand, and to evaporate. The change in the state of the refrigerant from liquid to gas causes energy (heat) to be absorbed. The refrigerant is recompressed from gas to liquid by the compressor. The heat absorbed by the evaporation stage and the heat produced during compression is expelled into the environment through a heat sink.

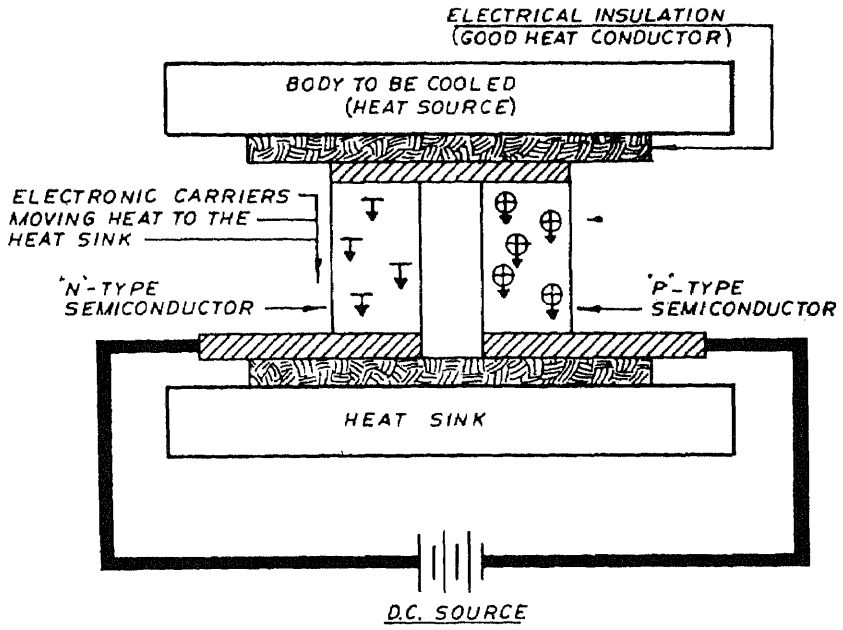

Figure 4.2 *A single thermoelectric element being bias by a DC source* [11].

The thermoelectric cooler essentially works in a similar fashion. Instead of refrigerant, electrons are used in case of the TEC (see Figure 4.2). At the cold side of TEC, energy (heat) is absorbed as electrons passes from a lower energy level of p-type material to a higher energy level of n-type material. At the hot side, the situation is reversed. Heat is emitted to the environment as electrons move from n-type high energy level to p-type low energy level. As shown in Figure 4.3, p-type and n-type semiconductor couples are placed electrically in series and thermally in parallel to make the device more effective.

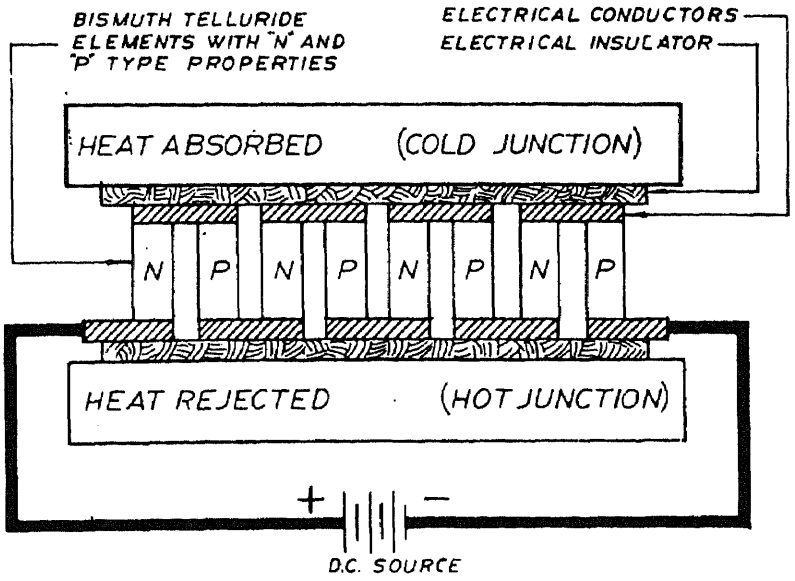

Figure 4.3 *Many thermoelectric elements connected in series electrically and in parallel thermally* [11].

Unlike the photon sensors, the microbolometer is a thermal sensor, and any change in the environment that the microbolometer is in can affect the temperature measurement. Therefore, the temperature inside the microbolometer packaging must be kept at a constant temperature. To accomplish this task, the thermoelectric cooler is used to stabilize the temperature inside the FPA packaging. The operation of thermoelectric cooler is controlled by the amount and the direction of current. Positive current (putting current into TEC) will heat up one side of the thermoelectric cooler and cools the other side of TEC, where the heat is removed from the cold side to the hot side. Negative current (pulling current out of TEC) will reverse the direction of the heat flow. The rate of heat being pumped from the cold side to the hot side is proportional to the amount of current passing through the thermoelectric cooler and the number of couples [11]. In the

case of microbolometer array, it will be most likely to be activated as a cooler due to heat buildup inside the array packaging during the process of imaging.

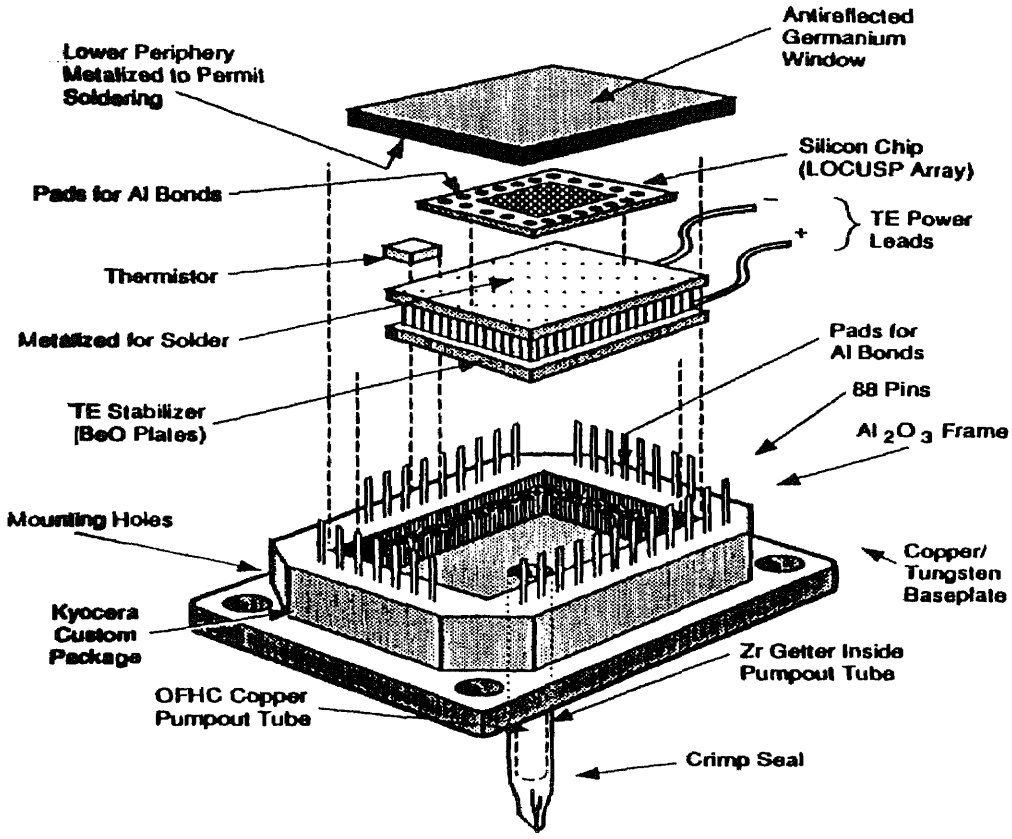

Figure 4.4 *Inside of a UFPA packaging* [8].

As shown in Figure 4.4, a thermoelectric cooler is placed underneath the microbolometer UFPA within the packaging. It will pump the heat from the inside of the package to the outside through back side conduction, which is attached to a heat sink.

4.2 The Controller Design

The controller is design to stabilize the temperature inside the vacuum array packaging to be at a constant temperature. A constant voltage is applied to the controller as a reference voltage that will determine the desired temperature inside the UFPA packaging. Figure 4.5 shows the block diagram of the controller loop. The output of the controller is connected to the pulse width modulator (PMW) of the switching power supply. The thermoelectric cooler is driven by the switching power supply to reduce the input power of the circuit.

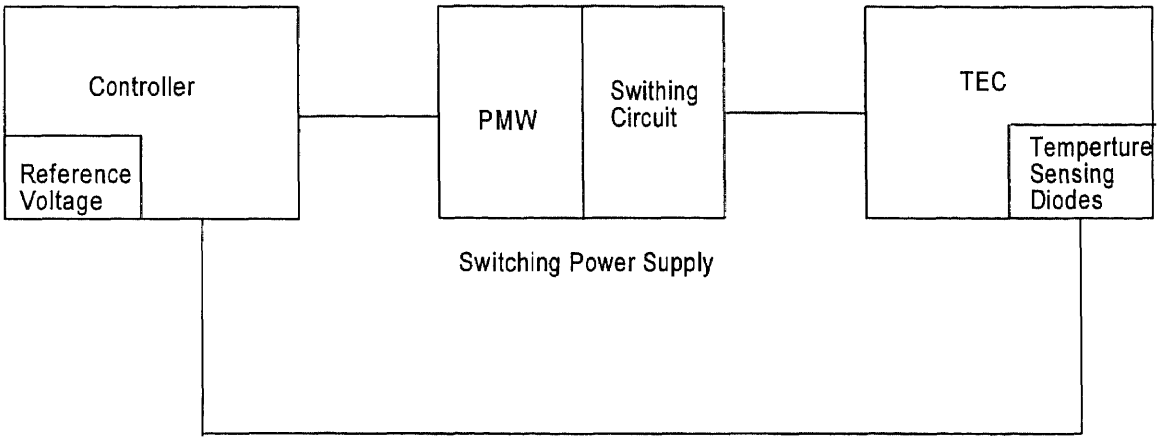

Figure 4.5 *A block diagram of the thermoelectric controller loop.*

The output power of the switching power supply is control by the pulse width modulator. The PWM produces pulses with frequency of around 20 KHz. The input to the PWM is from -5V to +5V , and the width of the pulses are determined by the input voltage. If the input voltage increases, the pulse width decreases and vice versa. The

switching circuit is a MOS step-down converter, which recycles the current produced by on-pulse during the off cycle of the pulses and converts the pulses to DC voltage to power the thermoelectric cooler.

As shown in Figure 2.13 and 4.4, there are two temperature sensors inside the packaging for the feedback to the thermoelectric cooler controller. The sensors are two npn transistors, where the base to emitter junction is used as a diode with temperature sensitivity of about -2.18 mV/°C. The diodes are connected in series to increase the output voltage of the diodes, where the sensitivity increases to -4.36 mV/°C. The controller circuit is to be able to stabilize minimum change in temperature of about 20mK. The temperature change translates to change in voltage of -4.36 mV/°C x 20mK = -87μV.

The operation of the control loop is as follows. If the temperature inside the packaging increases, the diode sensors' voltage drop. The voltage drop is compensated by the control amplifiers. The output of the controller circuit produces a negative pulse causing the PWM to increase the pulse width allowing the power supply to draw more current out of the TEC, which enables the TEC to pump more heat out from the array packaging. If the temperature decreases, the same procedure follows. Now, the output of the controller is a positive pulse, which decreases the pulse width of the PWM. The decrease in the pulse width causes the power supply to draw less current out, thus the TEC warms up.

The first step in designing the controller was to determine the transfer function of the TEC/diode pair (refer to as "TEC pump" in the thesis). An experiment was

performed at Inframetrics to determine the step response of the TEC pump. The temperature sensing diodes were connected as shown in Figure 4.6. The two diodes were connected in series and biased with 102KΩ resistor from +5 volts with current of about 40μA. The output of the diodes were connected to an oscilloscope to measure the step response of the TEC pump due to heating and cooling of the thermoelectric pump.

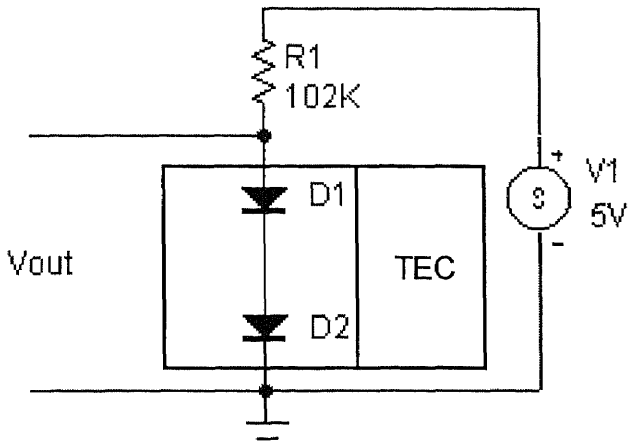

Figure 4.6 *The setup for determining the diode response.*

The thermoelectric cooler was connected to a power supply, and the step input was simulated by turning on the power supply. The oscilloscope was set to trigger on the rising edge of the input pulse to record the response data. Figure 4.7 shows the resulting response curves of the TEC pump, where the vertical scale represents the output voltage of the temperature sensors (diodes) and the horizontal scale represents time. In Figure 4.7 a), the TEC was cooled without a heat sink.

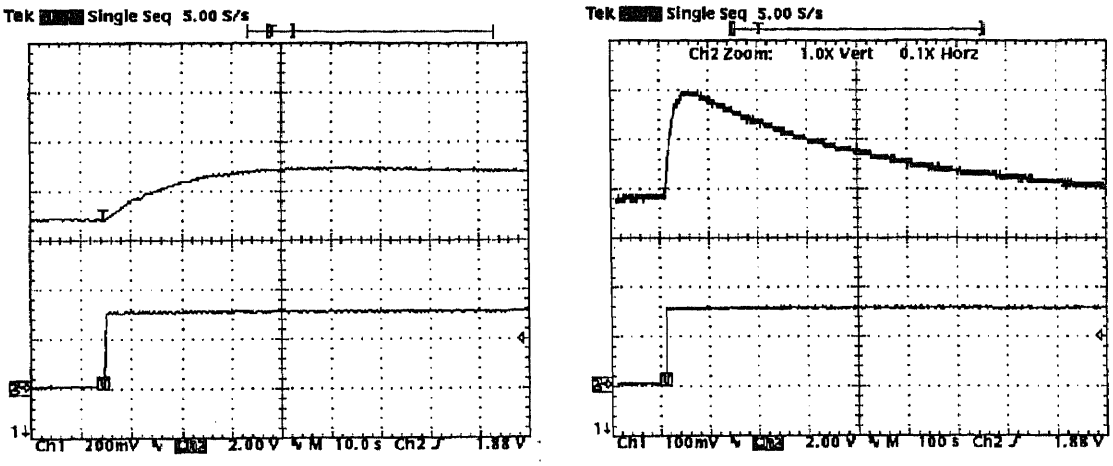

a) *Cooling the TEC without heat sink.*

Left: Vertical scale is 200mv/block for the upper curve, 2v/block for the lower curve, and 10s/block time scale.

Right: Vertical scale is 100mv/block for the upper curve, 2v/block for the lower curve, and 100s/block time scale.

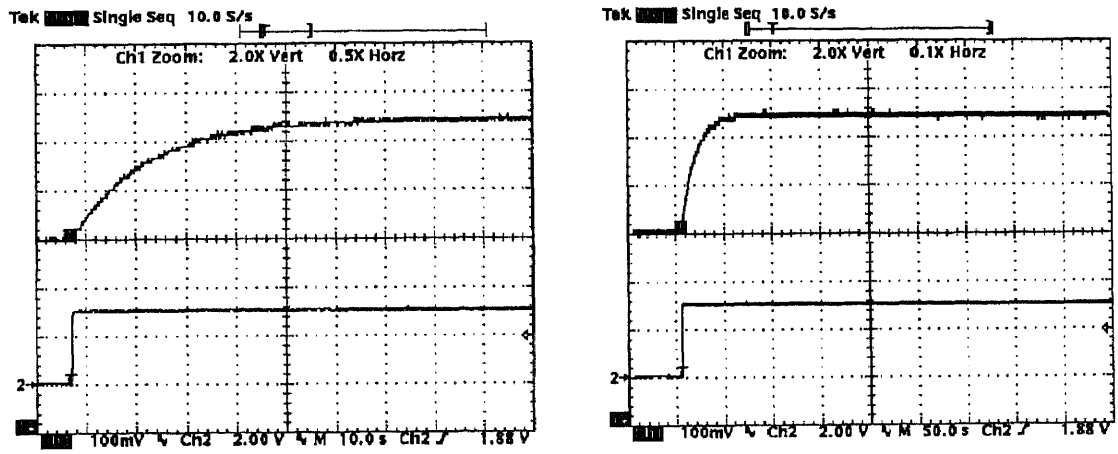

b) *Cooling of the TEC with heat sink.*

Left: Vertical scale is 200mv/block for the upper curve, 2v/block for the lower curve, and 10s/block time scale.

Right: Vertical scale is 100mv/block for the upper curve, 2v/block for the lower curve, and 50s/block time scale.

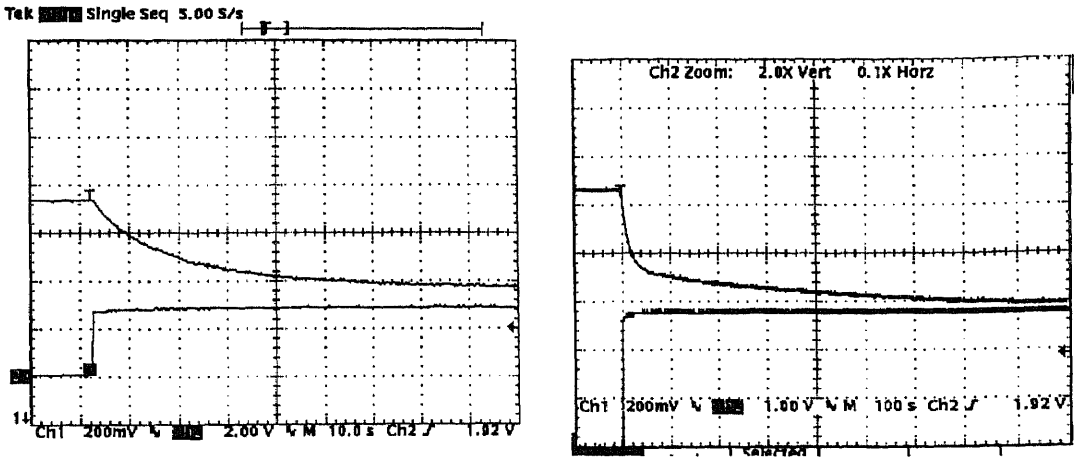

c) *Heating of the TEC without heat sink.*

Left: Vertical scale is 200mv/block for the upper curve, 2v/block for the lower curve, and 10s/block time scale.

Right: Vertical scale is 200mv/block for the upper curve, 1v/block for the lower curve, and 100s/block time scale.

Figure 4.7 *Step response of the TEC pump due to heating and cooling, where the vertical scale represents the output of the diodes and the horizontal scale represents time.*

As seen on the 100s/block time scale curve, the absence of the heat sink resulted in temperature increase inside the UFPA packaging (diode voltage drops) due to heat build up inside the packaging. In 4.7 b), the presence of the heat sink stabilized the temperature. In Figure 4.7 c), the effect of heating can be observed.

As observed from the step response curves, the TEC pump has a time constant of about 20 seconds. An equivalent electrical circuit model was derived from the curves (Figure 4.8). The model is in the simplest form, and there are other more complex models. As shown in Figure 4.9, the model has a time constant of 20 seconds. The value

of the resistors and the capacitor is chosen to match the input and output impedance of the TEC pump.

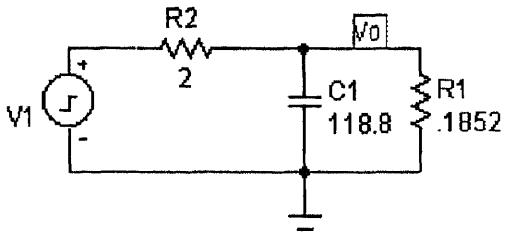

Figure 4.8 *The equivalent circuit of the TEC pump model.*

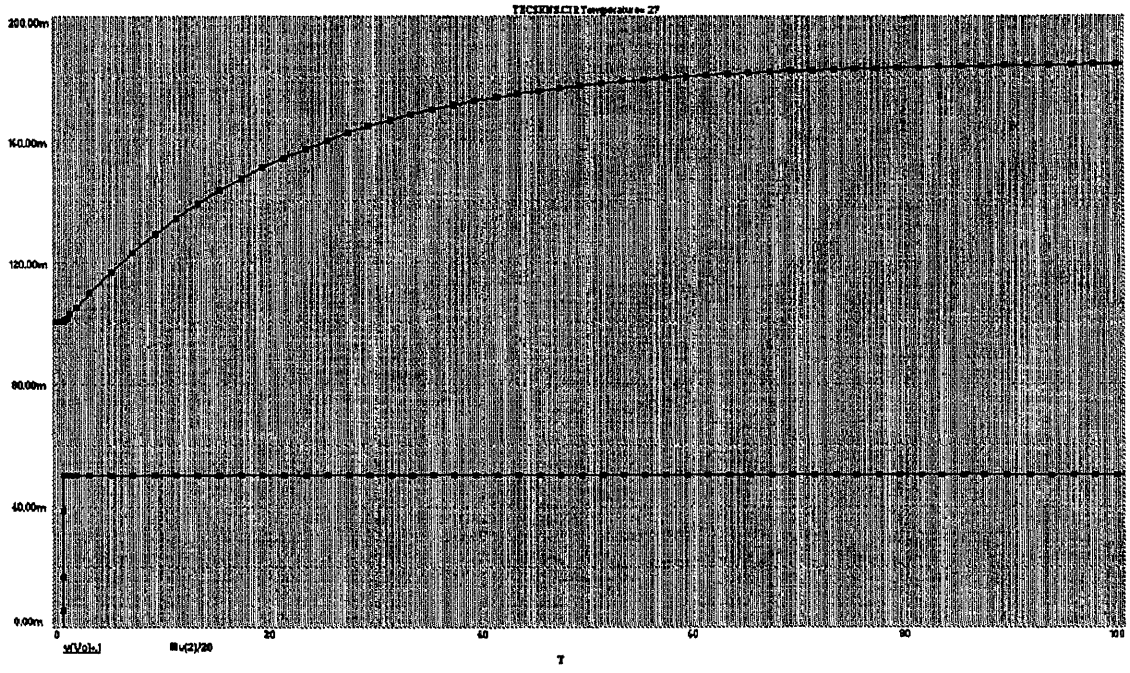

Figure 4.9 *Step response of the equivalent TEC pump model.*

Using the equivalent model, the transfer function, $H_m(s)$, of the TEC pump model was derived.

$$H_m(s) = \left[\frac{(R_1 R_2 C_1)s + (R_1 + R_2)}{(R_1 C_1)s + 1} \right] \tag{4.1}$$

Pole of the function is solved by setting the denominator equal to zero,

$$-\frac{1}{R_1 C_1} = -0.04545. \tag{4.2}$$

Similarly, zero of the transfer is determined as

$$-\frac{R_1 + R_2}{R_1 R_2 C_1} = -0.049785, \tag{4.3}$$

and the pole and zero of the equation are plotted in Figure 4.12 c).

Based on the transfer function the TEC pump model, the thermoelectric controller circuit (Figure 4.10) was designed. The controller is a lag compensator with a differential gain. The controller circuit configuration was chosen due to its flexibility of positioning poles and zeros of the controller, easily adjustable for the complex TEC pump models, without losing gain control.

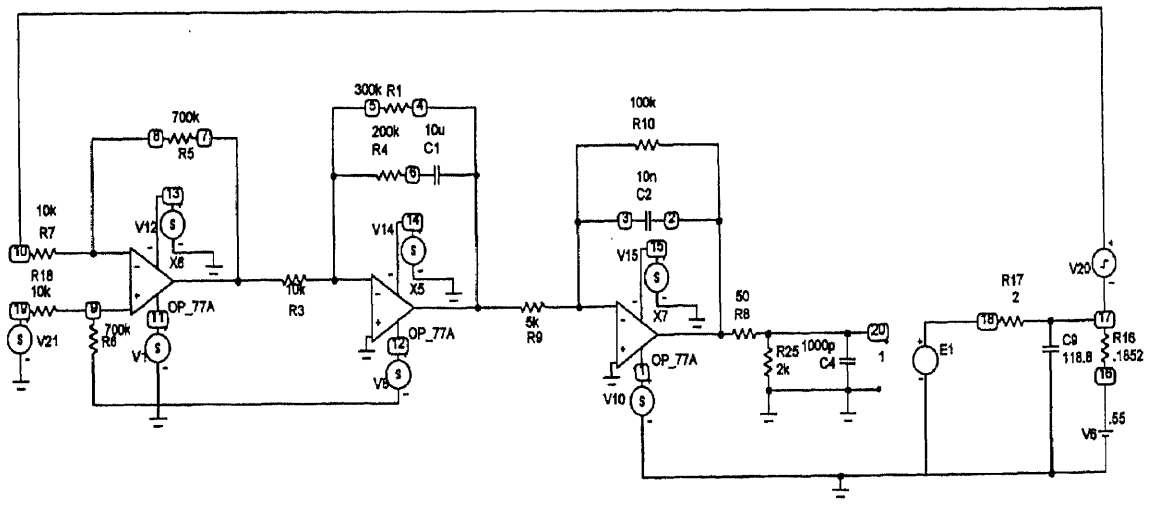

Figure 4.10 *The thermoelectric cooler controller circuit schematic.*

The controller configuration was first used as a linear power supply TEC controller at Inframetrics. With the use of the root locus plots and the circuit response simulation, modification was made to the resistor and the capacitor values of the controller circuit to optimize it for the TEC pump model and the switching power supply circuit.

The first three op-amps represent the controller, and the dependent voltage source in the circuit is placed after the controller to drive, in the place of switching power supply, the TEC pump model circuit. The pulse source is placed in the feedback path to simulate the TEC temperature fluctuation, and the pulse is fed to the negative terminal of the differential amplifier. The reference voltage is fed to the positive terminal.

Root locus of the circuit was plotted to predict stability and response of the circuit using Matlab. The following equations are the open loop transfer function of the each amplifier stage of the controller. $H_1(s)$, $H_2(s)$, and $H_3(s)$ refer to the differential amplifier stage, the second amplifier stage, and the third amplifier stage transfer functions, respectively. The differential amplifier only has a DC gain.

$$H_1(s) = \frac{R_5}{R_7}; \tag{4.4}$$

DC gain: 70

The second amplifier has the following characteristics:

$$H_2(s) = -\frac{R_1}{R_3}\left[\frac{(R_4C_1)s+1}{((R_1+R_4)C_1)s+1}\right]; \tag{4.5}$$

DC gain: -30

$$\text{Zero: } -\frac{1}{R_4C_1} = -0.5 \tag{4.6}$$

$$\text{Pole: } -\frac{1}{(R_1+R_4)C_1} = -0.2 \tag{4.7}$$

The third amplifier stage has the following characteristics:

$$H_3(s) = -\frac{R_{10}}{R_9}\left[\frac{1}{((R_{10}C_2)s+1}\right]; \tag{4.8}$$

DC gain: -20

$$\text{Pole: } -\frac{1}{R_{10}C_2} = -1000 \tag{4.9}$$

The pole was place far to the right of the imaginary axis for fast response time. Multiplying all the DC gains, the circuit has an overall gain of 70 x -30 x -20 = 42000. The value of the gain was necessary for the small voltage (80μV) compensation and to ensure the cancellation of the poles and zeros. The poles and zeros are plotted in Figure 4.12 a) and b).

Figure 4.12 a) shows the overall view of the pole-zero locations on the s-plane. The cancellation of the amplifier pole and zero with the circuit gain of 42000 can be seen in Figure 4.12 b). Figure 4.12 c) is the view of the root locus plot of the TEC pump model. With the gain of the circuit, the pole and zero canceled each other out.

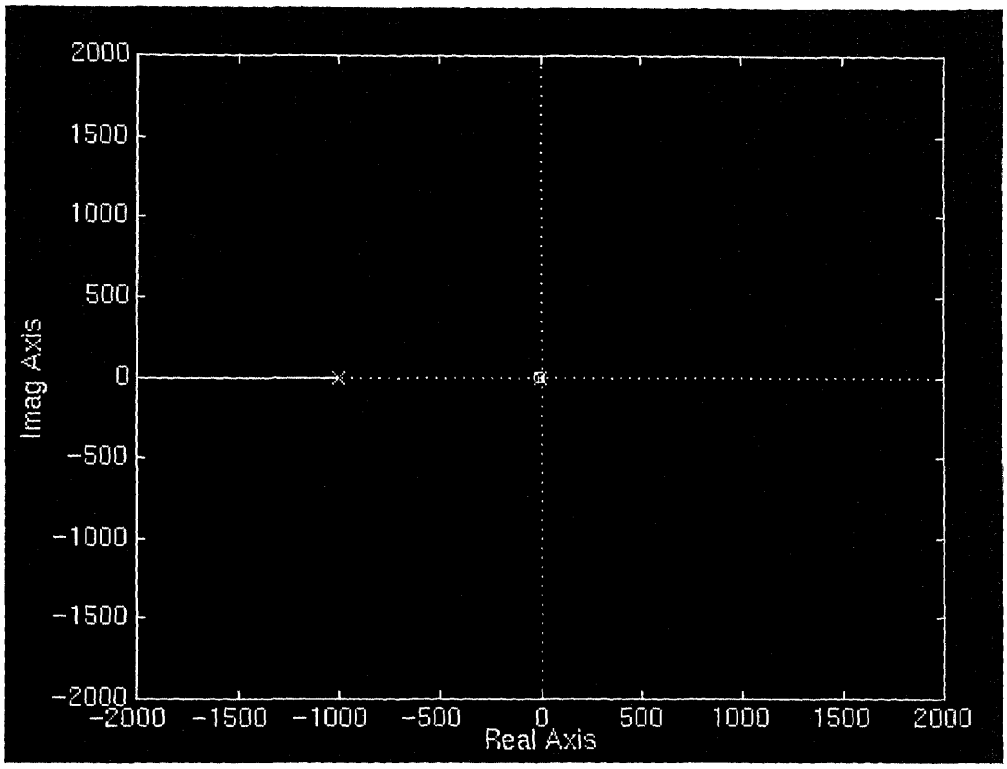

a) *Overview of the root locus plot.*

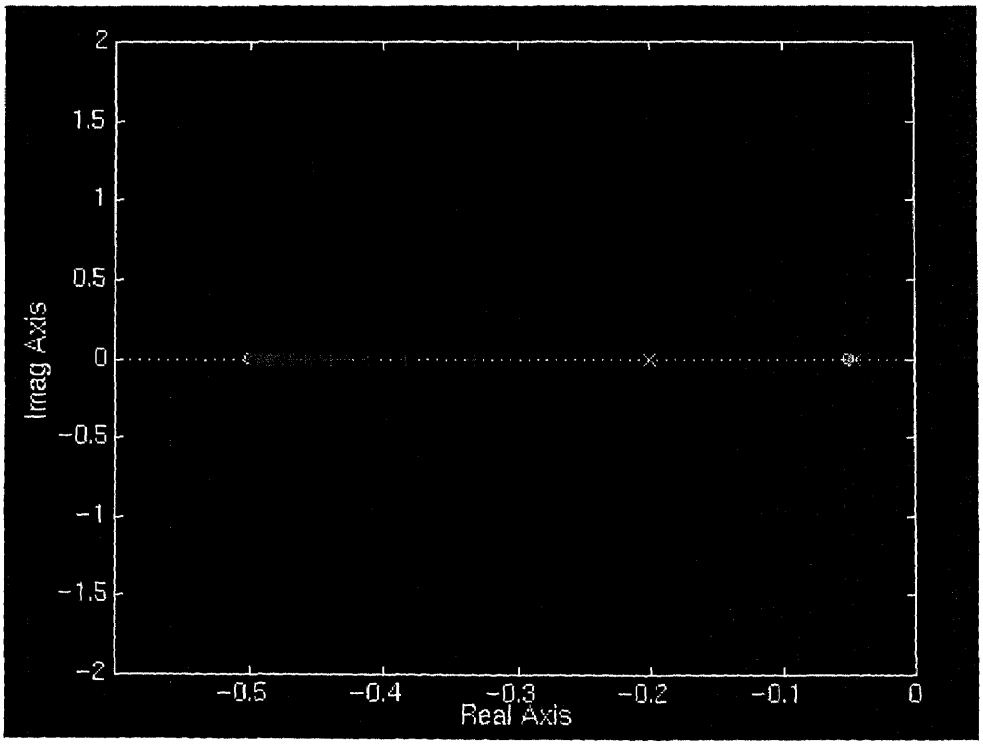

b) *Zoomed view of the root locus plot.*

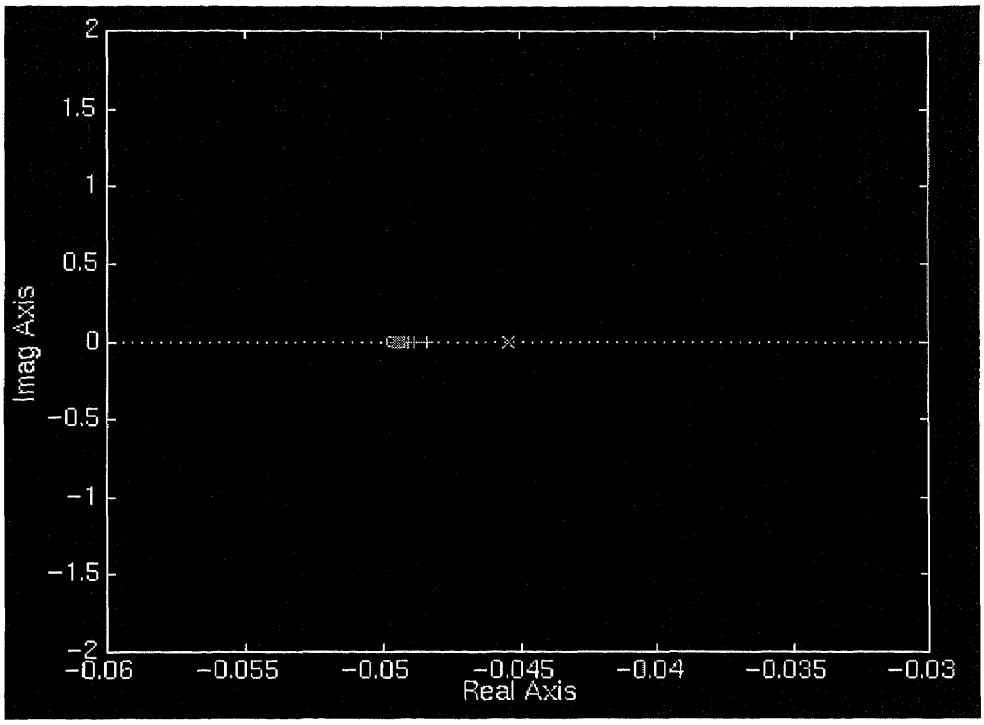

c) *Zoomed view of the pole and zero of the TEC pump model.*

Figure 4.12 *Root locus plot of the control loop with gain of 42000.*

The circuit simulation was done on Micro-Cap V. The pulse source in the feedback path was set to rise to -80μV at 1 second, simulating the 20mK temperature change in the UFPA packaging. The reference voltage was set at 0.5 volts in the simulation. Figure 4.11 (see delta) shows the circuit response to -80μV input, where the initial output voltage v(10) is at 0.5V. As seen from Figure 4.11 b) and c) (looking at the output voltage v(10)), the circuit achieved stability in about 30 ms to the -80μV disturbance.

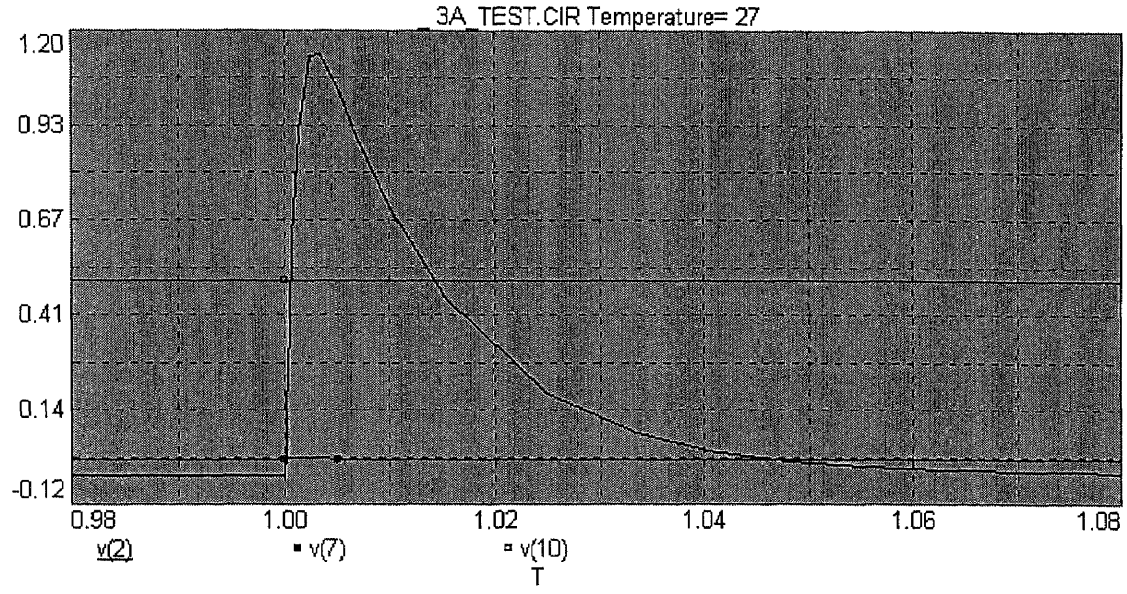

a) *The output response.*

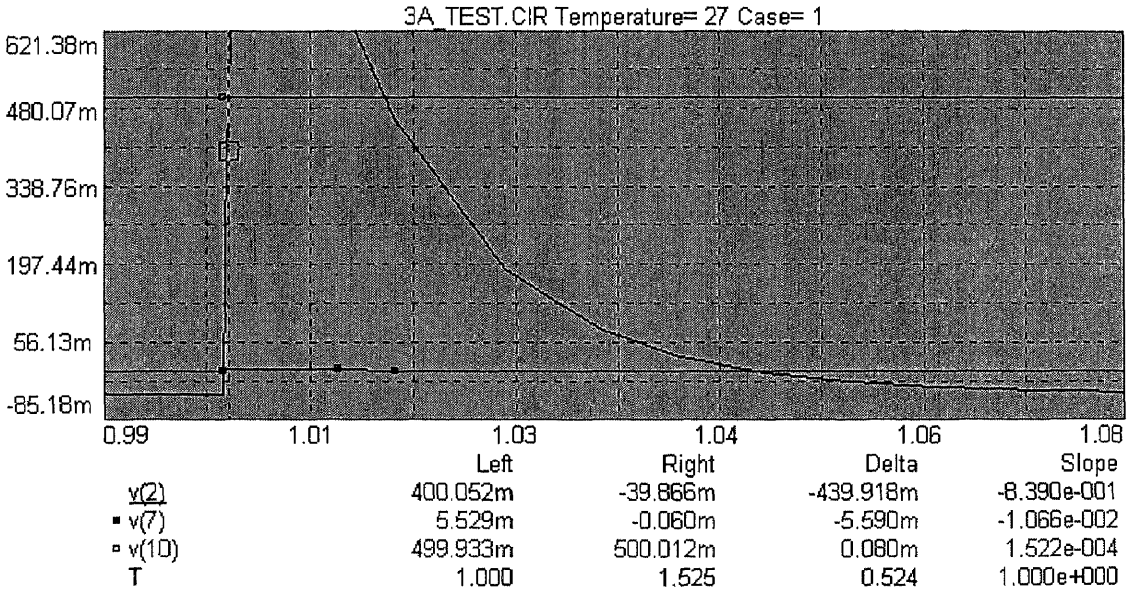

b) *v(10) showing the 80μV step voltage.*

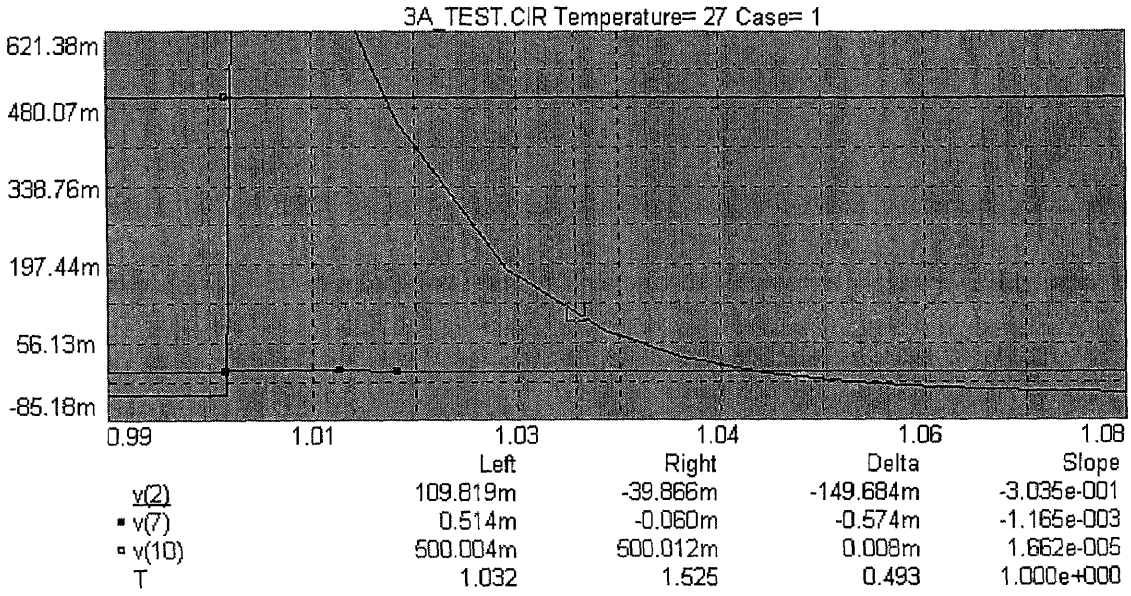

c) T *showing the response time of about 30ms.*

Figure 4.11 *Response of the controller circuit due to -80μV disturbance.*

CHAPTER 5

CONCLUSION

In this thesis, the ULTRA project uncooled microbolometer camera system was analyzed. The Rockwell U3000 microbolometer UFPA and Inframetrics' camera hardware and software were described and the theory of microbolometer was mathematically illustrated. In addition, the performance parameters (responsivity, NETD, and noise) of the focal plane array and the operation of the U3000 chip was described. The Inframetrics' camera hardware and software features and process was also described.

For the second part of the thesis, the thermoelectric cooler controller was designed and simulated. The model of the TEC pump was created from the experiment. According to the model, the controller circuit was designed by the lag compensator technique. The design included simulation in Matlab and Micro-Cap V. Matlab was used to determine the root locus plot of the control loop, and Micro-Cap V was used to simulate the circuit response to -80μV step input, where the voltage simulated the 20mK temperature change induced on the TEC pump. The circuit responded with about 30ms response time to the 80μV step input.

As follow up to this research, the controller should be simulated with the complex version of TEC pump model, and the circuit should be built and tested with the actual array packaging.

REFERENCES

1. R. A. Wood, "Uncooled Thermal Imaging with Monolithic Silicon Focal Planes", *SPIE Proc.,* Vol. 2020, 1993.

2. R.A. Wood, B. E. Cole, C. J. Han, R. Higashi, etc., "HIDADA Monolithic, Silicon, Uncooled Integrated Imaging Focal Plane Array," 17th *Government Microcircuit Applications Conference*, 1991.

3. P. W. Kruse, "Uncooled IR Focal Plane Arrays," *Infrared Technology XXI*, Vol. 2552, 1995.

4. P. W. Kruse, "Uncooled IR Focal Plane Arrays," *SPIE Proc.,* Vol. 2552, 1993.

5. R. J. Herring, P. E. Howard, "Design and Performance of the ULTRA 320 x 240 Uncooled Focal Plane Array and Sensor", *SPIE Proc.,* Vol. 2746, 1996.

6. P. W. Kruse, "Design of Uncooled Infrared Imaging Arrays", *SPIE Proc.,* Vol. 2746, 1996.

7. P. W. Kruse, *Elements of Infrared Technology,* Wiley, New York, 1962.

8. C. A. Marshall, N.R. Bultler, R. Blackwell, R. Murphy, T. Breen, "Uncooled Infrared Sensors with Digital Focal Plane Array", *SPIE Proc.,* Vol. 2746, 1996.

9. P.W. Kruse, "Uncooled IR Focal Plane Arrays," *SPIE's International Symposium on Optical Science, Engineering, and Instrumentation* , July 1995.

10. P. E. Howard, C. J. Han, J. Stevens, E. J. Clarke, "GENII 320x240 TV Compatible VOx Microbolometer UFPA," Rockwell, June 1996.

11. MELCOR Thermoelectric Cooler manual.